

X-Band Phased Array Antenna Validation Report

March 1, 2002

Kenneth Perko
*NASA Goddard Space Flight Center
Greenbelt, Maryland 20771*

Raymond Huggins, Peter Heisen, Gary Miller, Donald McMeen
*Boeing Phantom Works
Seattle, Washington 98055*

Tom Dod
*Swales Aerospace
Beltsville, Maryland 20705*

John Staren, Victor Sank, Xuan Nguyen
*QSS Group, Inc.
Greenbelt, Maryland 20770*

NASA/GSFC

Table of Contents

1.	INTRODUCTION.....	1
2.	TECHNOLOGY DESCRIPTION	2
2.1	XPAA Description.....	2
2.2	EO-1 X-Band System Description.....	5
3.	TECHNOLOGY VALIDATION.....	7
3.1	Brief Development and Flight History	7
3.2	Validation Overview and Results	8
3.3	EO-1 XPAA Link Error Performance	9
3.3.1	Introduction.....	9
3.3.2	Phased Array Antenna Characteristics.....	9
3.3.3	Link Characteristics	9
3.3.4	Test Procedures.....	10
3.3.5	Data Collection	10
3.3.6	Data Analysis	11
3.3.7	Results.....	12
3.3.8	Burst Error Statistics	12
3.3.9	Periodic Errors	13
3.3.10	Conclusion	18
3.4	EO-1 XPAA Antenna Pattern/Scan Performance.....	18
3.4.1	Introduction.....	18
3.4.2	Anechoic Chamber Patterns and Near Field Scans Prior To Launch.....	18
3.4.3	Integration and Test Results.....	20
3.4.4	On-Orbit Tests Using Ground Stations.....	23
3.4.5	Antenna Pattern Results.....	23
3.4.6	Scan Performance Results.....	25
3.5	Validation of the Performance and Reliability of the Electronics and Software	26
4.	TECHNOLOGY TRANSFER AND INFUSION POTENTIAL.....	29
5.	LESSONS LEARNED.....	29
6.	CONTACT INFORMATION	30
7.	VALIDATION SUMMARY	30
8.	ACKNOWLEDGEMENTS	30
9.	REFERENCES.....	31
	ACRONYMS and ABBREVIATIONS.....	32
	Appendix A - EO-1 Quadrature Differential Design (Gray code).....	33
	Appendix B – Distribution of Errors Per Bin	34
	Appendix C – EO-1 X-Band Link Budgets	35
	Appendix D – EO-1 X-Band Coordinate Reference Frames.....	36

List of Illustrations

Figure 1. Exploded view of EO-1 spacecraft indicating the location of the XPAA at the end of a boom on the nadir-facing panel.	1
Figure 2. Photograph of the XPAA prior to spacecraft integration	2
Figure 3. Photograph of RSN board prior to insertion in XPAA housing	3
Figure 4. XPAA block diagram	4
Figure 5. EO-1 X-band system configuration diagram.....	6
Figure 6. XPAA and test hood during integration with EO-1 spacecraft.	6

Figure 7. Ground Station Configuration	10
Figure 8. XPAA Burst Error Statistics	13
Figure 9. Error Histogram (1)	14
Figure 10. Error Histogram (2)	14
Figure 11. Error Histogram (3)	15
Figure 12. Error Histogram (4)	15
Figure 13. Error Histogram (5)	16
Figure 14. Errors Per Bin Distribution (1)	17
Figure 15. Errors Per Bin Distribution (2)	17
Figure 16. Errors Per Bin Distribution (3)	18
Figure 17. Post-delivery tests of the XPAA using the NSI near field scanner at Swales Aerospace.	19
Figure 18. Near field scanning the XPAA after integration with EO-1 at GSFC. This setup was also used for the final EIRP measurement before EO-1 was shipped to the launch site.	20
Figure 19. Comparison of pattern calculated using NF data taken at GSFC (red) with the equivalent Boeing anechoic chamber pattern ($\alpha = 0$, $\beta = 0$).....	21
Figure 20. Comparison of pattern calculated using NF data taken at GSFC (red) with the equivalent Boeing anechoic chamber pattern ($\alpha = 45$, $\beta = 0$).....	21
Figure 21. Calculated XPAA contour plots from near field measurements taken at Boeing prior to delivery, at Swales before integration with EO-1, and after integration.....	22
Figure 22. Near field data showing the calculated amplitude (top) and phase (bottom) distributions across the aperture of the XPAA when pointed to $\alpha=0$, $\beta=0$ (left) and $\alpha=45$, $\beta=315$ (right).....	22
Figure 23. Example of EO-1's X-band frequency-domain spectrum that was recorded with the "Specviewer" program (left) and the resultant time- domain Excel plot of XPAA emitted power from "Specdata" corrected for range variations during the pass (right). The XPAA was pointed to boresight throughout the pass.	23
Figure 24. Antenna pattern cut taken from orbit as EO-1 passed over GSFC. Angles are shown in degrees (large divisions = 20 degrees).....	24
Figure 25. Antenna pattern from EO-1 after launch, adjusted for range and path losses, compared to equivalent cut derived from pre-launch near field measurement data.	25
Figure 26. Predicted and actual signal-to-noise ratios at the Wallops ground station during an EO-1 pass. The predicted level includes adjustments for slant range and EIRP variation of the XPAA due to scan angle.....	26
Figure 27. Power supply voltages associated with the Essential Services Node (ESN) processor before, during, and after a downlink event.	27
Figure 28. Power supply voltages associated with the XPAA's RF modules before, during, and after a downlink event. These supplies are operative only during actual downlinks.....	27
Figure 29. Power supply currents associated with the XPAA's RF modules before, during, and after a downlink event. These currents are drawn only during actual downlinks. The negative currents are for bias circuits. The positive currents vary with the antenna's pointing angle due to array effects on the elements.	28
Figure 30. XPAA internal temperatures before, during, and after a downlink event.	28

List of Tables

Table 1. Noise Injection Parameters	11
Table 2. BER Data Sets	12
Table 3. Error Histogram Statistics.....	16
Table A-1. EO-1 Gray Code and Quadrature Differential Encode Format	33

1. INTRODUCTION

Earth Observing-1 (EO-1) is the first satellite in NASA's New Millennium Program (NMP) Earth Observing series. While EO-1's primary focus is to develop and test a set of advanced technology land imaging instruments, many other key supporting technologies are demonstrated as a part of the mission. Demonstration of these technologies by EO-1 is intended to reduce the cost, mass, and complexity of future Earth observing spacecraft, allowing a higher percentage of a future mission's mass to be devoted to the scientific payload.

In particular, the EO-1 mission provides for the on-orbit demonstration of a high data rate, low-mass X-band Phased Array Antenna (XPAA) for returning to ground the imaging data stored in the EO-1 solid-state recorder. The XPAA combines the functions of antenna, 2-axis gimbal, gimbal controller, and solid-state power amplifier (SSPA) in a single, low-cost package. Phased array technology offers significant benefits over mechanically pointed parabolic antennas, including the elimination of deployable structures, moving parts, and the torque disturbances that moving antennas impart to the spacecraft. The latter feature results in the conservation of spacecraft power and enables the ability to take precision optical measurements while simultaneously transmitting high-rate data. The division of the SSPA function into 64 individual element amplifiers enhances the reliability and fault tolerance of the X-band downlink system. Figure 1 shows an exploded view of the EO-1 spacecraft and illustrates the location of the XPAA.

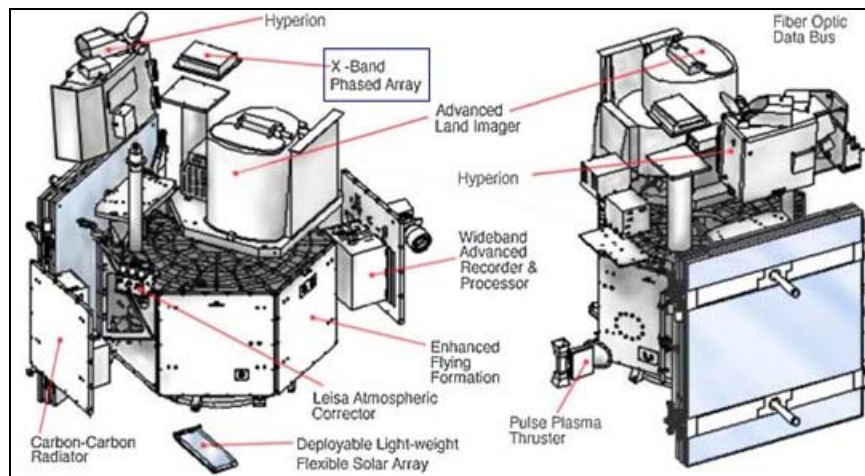


Figure 1. Exploded view of EO-1 spacecraft indicating the location of the XPAA at the end of a boom on the nadir-facing panel.

These antennas are seen as particularly applicable to NASA's new generation of small yet highly capable science spacecraft. NASA has not previously flown phased arrays of this type for high data-rate downlink applications.

The antenna operates at a frequency of 8225 MHz, transmits data at 105 Mbps with minimum effective isotropic radiated power (EIRP) at 22 dBW, has an integral controller and power conditioner, communicates with the spacecraft over a MIL-STD-1773 fiber-optic data bus, and is fully space qualified. The nominal mission life for EO-1 was one year, and the original operational requirement was for one 10-minute transmission per day to an 11-meter ground station antenna at high latitudes in the Northern Hemisphere, either Spitsbergen, Norway, or Alaska.

The phased array technology flown on EO-1 was designed and built by Boeing's Phantom Works in Seattle, Washington. The antenna was integrated to EO-1 at the Goddard Space Flight Center (GSFC) in Greenbelt, Maryland, where final performance tests were made. EO-1 was launched from Vandenberg AFB in California in November 2000.

The XPAA has performed flawlessly since launch. After some initial difficulty with NASA ground station configurations for the X-band downlink, EO-1 is currently returning more than 160 Gigabits of science telemetry to Earth daily using the XPAA.

The GSFC Microwave Systems Branch managed development and validation of the XPAA for the EO-1 project. Details of the antenna and its performance during the mission are described in this paper.

2. TECHNOLOGY DESCRIPTION

2.1 XPAA Description

The antenna aperture consists of an 8 x 8 array of modules, each comprising a dielectrically loaded, circular waveguide, two orthogonal antenna feeds, a phase shifter, and a dual power amplifier. The modules are arranged in an equilateral triangle lattice with the module spacing selected to prevent the onset of grating lobes at the maximum scan angle of 60 degrees. The array is excited uniformly in amplitude. A multiple layer wide-angle impedance matching (WAIM) radome is incorporated into the aperture design to provide a nearly ideal cosine scan behavior to 60 degrees of scan over all azimuth angles. The WAIM design also provides for a low polarization axial ratio over the array's scan volume. The radiation is left-hand circularly polarized.

The 64 modules are mounted in a printed wiring board, which distributes radio frequency (RF) excitation, logic control signals, and power to each module. The array receives power and logic control signals from the Remote Services Node (RSN) controller board. Prime power to the RSN is 28 +/- 7 volts-DC (VDC) from the spacecraft bus, and commands are transmitted over a MIL-STD-1773 fiber-optic bus. Command signals (elevation angle (θ), azimuth angle (ϕ), $d\theta/dt$, and $d\phi/dt$) are transmitted to the antenna from EO-1's attitude control system once every second. The array and RSN are located in a single 12 x 13 x 2.9-inch enclosure with a total mass of 5.5 kg. Figure 2 presents a photograph of the XPAA prior to spacecraft integration.

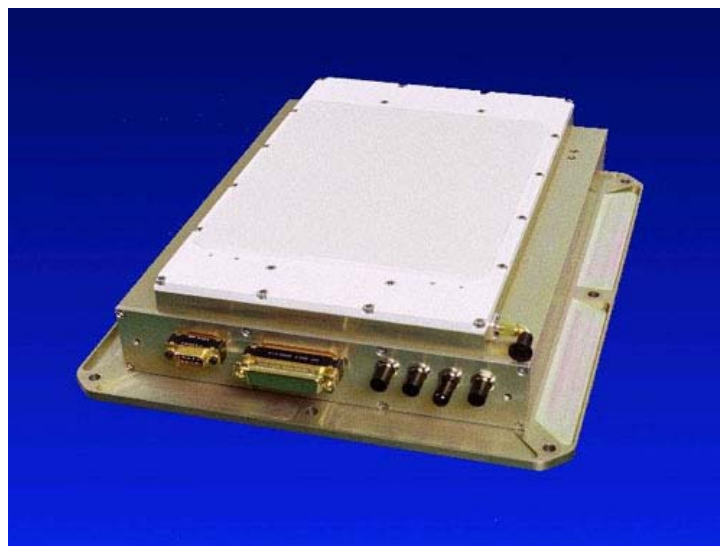


Figure 2. Photograph of the XPAA prior to spacecraft integration.

The RSN is a generic controller built by Litton Amecom, which is customized for the different instruments on the EO-1 satellite by the addition of specific electronic components. The generic board contains a multichip module (the Essential Services Node or ESN) fabricated by Honeywell, and two dual rate 1773 transceivers operating at 1 MHz fabricated by Boeing. The ESN comprises a processor and both analog and digital input/output (I/O) devices. Custom electronic components for the X-band antenna controller includes an FPGA, output buffers, and six Interpoint dc-to-dc converters. A block diagram showing the overall configuration is given in Figure 4. As can be seen in the photographs of the array and the RSN in Figures 2 and 3, the dimensions of the RSN and its mounting scheme drove the size and footprint of the XPAA.

The ESN program code is stored in an Electronically erasable programmable read only memory (EEPROM) and is loaded via an external port. In addition to managing the RSN and encoding and decoding data for transmission over the 1773 data bus, the program also performs the following functions:

- Calculation of the four-bit phase values for each module based on its location in the array, the commanded pointing vector (θ and ϕ), the rates $d\theta/dt$ and $d\phi/dt$, and the elapsed time.
- Loading the 256-bit phase information into an output buffer.
- Clocking the phase information out to the array at an update rate of 2 per second.
- Collection of housekeeping data and its transmission to the spacecraft over the 1773 data bus.

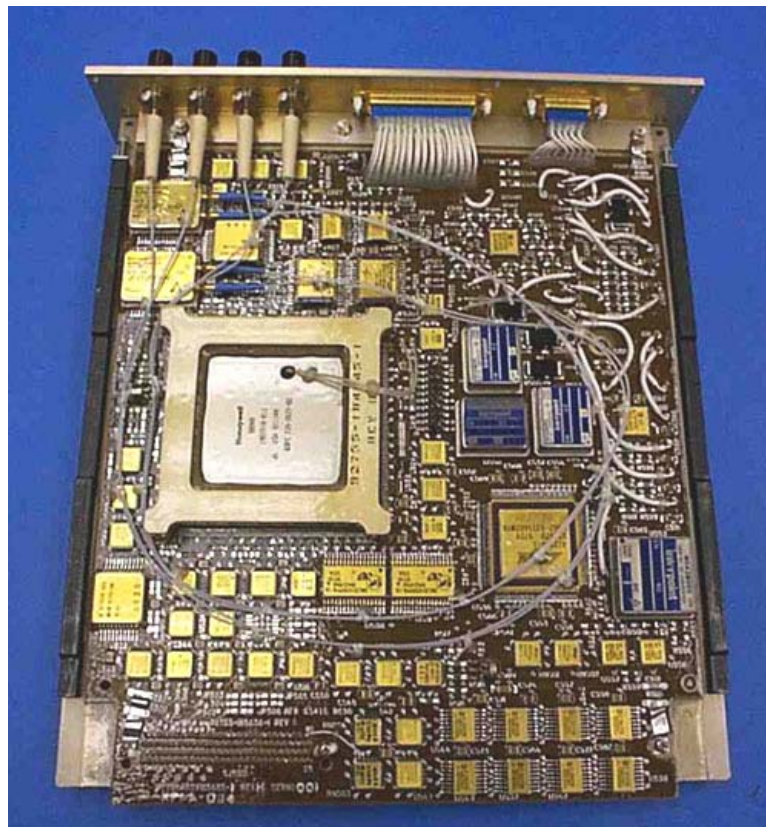


Figure 3. Photograph of RSN board prior to insertion in XPAA housing.

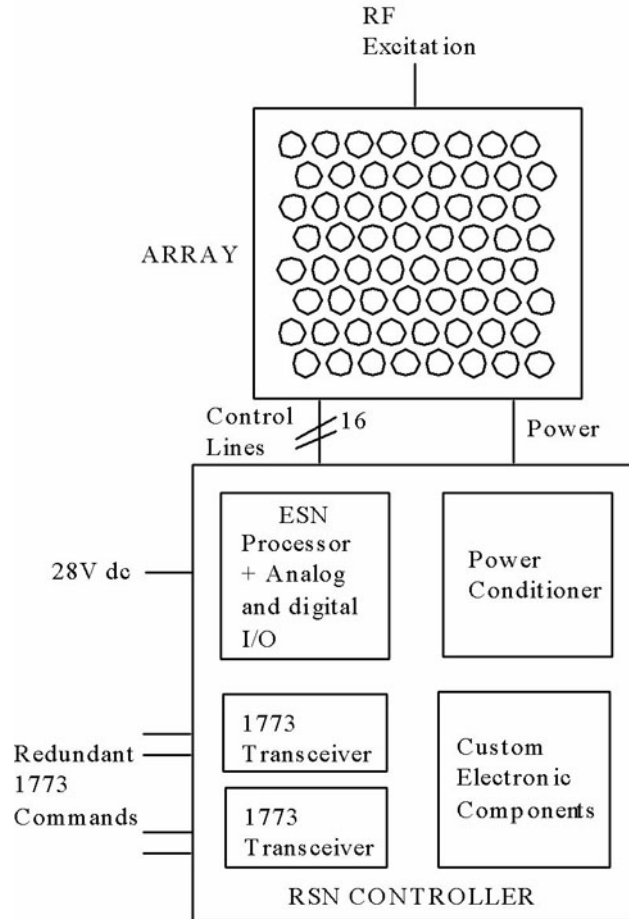


Figure 4. XPAA block diagram.

Each of the 64 RF modules contains three monolithic microwave integrated circuits (MMICs) (a 16-step (4-bit) phase shifter, a driver amplifier, and a dual power amplifier), and an application-specific integrated circuit (ASIC) controller. The two outputs from the dual power amplifier drive two antennas, which launch RF power into the circular waveguide. The two signals are 90 degrees out of phase giving a circular polarization. The integrated circuits are mounted on a ceramic chip carrier on the base of the module with fingers on the ceramic carrier lining up with fingers on the printed wiring board. Contact between the two is made via an elastomeric connector. At the 1-dB compression point, the average module gain was 22 dB, the power output was 18 dBm (decibel-milliwatts), and the power added efficiency (PAE) was 22%. The size of each module is approximately 0.7 inch in diameter and 0.5 inch long. The drive to the antenna is set so that the 22dBW EIRP minimum requirement is achieved at maximum scan angle of 60°.

Radiation effects are a concern in low-Earth-orbit. The ASIC controller was not radiation hardened, and was tested for total ionizing dose (TID) and single event latch-up (single event upsets are not a concern since the pointing commands are updated every half second, and a single module upset would have little effect on the antenna performance). The tests showed that the threshold TID for impaired functionality was ~3 kilo-Rads in Silicon (krad(Si)) (neglecting annealing effects). Degradation occurs only when the ASIC is biased, and for 10 minutes/day for one year, the total dose was been estimated to be ~ 2.4 krad(Si). The TID for the nominal life of the mission is therefore not a problem. A Single Event Latch-up (SEL) is however a concern as test data and predicted radiation levels showed that the possibility of a SEL for one of the 64 modules for the life of the mission is ~3%. An SEL can result in a normally high impedance transistor, in the ASIC, turning on

like a silicon-controlled rectifier (SCR) and thereby possibly shorting the positive supply rail to ground. To eliminate the possibility of damage to the ASIC and permanently shorting the supply voltage to ground, a $1\text{k}\Omega$ series resistor was placed in the ASIC V_{cc} line in each module.

One feature of the software is that in the absence of any signal on the 1773 data bus for two minutes, the antenna points to boresight ($\theta = 0$ degrees and $\phi = 0$ degrees), and turns on the RF amplifiers. The antenna then functions similarly to a fixed dish. While this feature was added to improve in-flight reliability of the RF downlink, it was a cause of some concern during spacecraft I&T, where 1773-bus interruptions were to be expected. At least one such extended interruption did occur, causing the antenna to activate this feature by accident.

2.2 EO-1 X-Band System Description

The X-band downlink was originally designed to provide a Landsat 7 equivalent link of 150 Mbps communications link to one or more NASA polar ground stations (9-meter or larger antennas) with substantial link margin. Early in EO-1's development, the decision was taken for the downlink to duplicate the characteristics of the Radarsat mission so that pre-existing ground station equipment for that satellite could be used. Radarsat used a 105-Mbps quadrature phase shift key (QPSK) downlink with Gray coding, which is described further in Section 3.3.3 and Appendix A. Therefore the final link margins achieved were even higher than intended. A major benefit of this was that the extra margin enabled EO-1 to conduct error-free downlinks to the GSFC 3-meter antenna at Greenbelt for some contingency and validation activities.

Since EO-1 would be spending the bulk of its mission in close proximity to Landsat 7, the downlink polarization was chosen to be left-hand circular. This ensured maximum interference isolation between the two spacecraft, since Landsat 7's polarization was right-hand. As it turned out, EO-1 is the only spacecraft serviced by the polar ground network to be left-hand polarized. This had undesirable consequences during early-orbit operations that are described in the following section.

A link budget is shown in Appendix C, illustrating the EO-1 link budgets as flown and as originally proposed.

The XPAA required an X-band modulated input signal of approximately 14 dBm to produce full 22 dBW EIRP at all scan angles. An RF exciter card that was contained in the Wideband Advanced Recorder Processor (WARP) enclosure provided this signal. Reed-Solomon encoded data to be downlinked (which was stored in the WARP) was supplied to the card as differential in-phase (I), quadrature (Q), and clock signals. The card provided Gray coding of the data and pre-modulation filtering. After filtering, the data was QPSK modulated on an 8225-MHz carrier and amplified to 18 dBm. This signal was conducted to the XPAA via a pair of coaxial cables, with an in-line attenuator added to allow fine-tuning of the drive level after all parts were integrated with the EO-1 spacecraft. A system configuration diagram is presented in Figure 5.

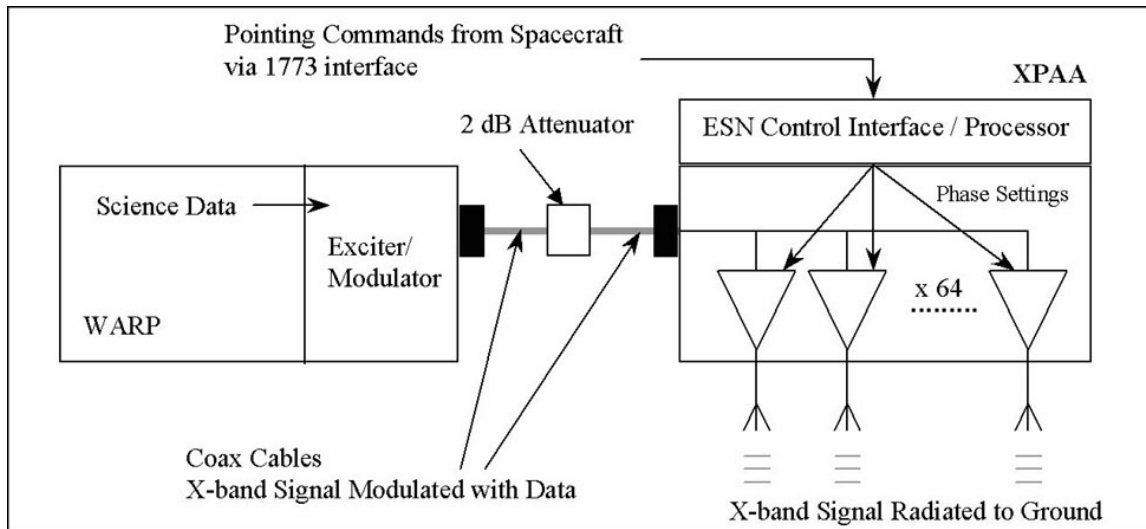


Figure 5. EO-1 X-band system configuration diagram.

During spacecraft integration and testing, a test hood (designed by Boeing and delivered as part of the contract) was placed over the antenna as shown in Figure 6. This enabled the XPAA to radiate safely in a laboratory environment. A small helix inside the hood collected an attenuated sample of the signal to enable verification of the output power and to allow 105-Mbps data to flow from the spacecraft via RF to ground support equipment.

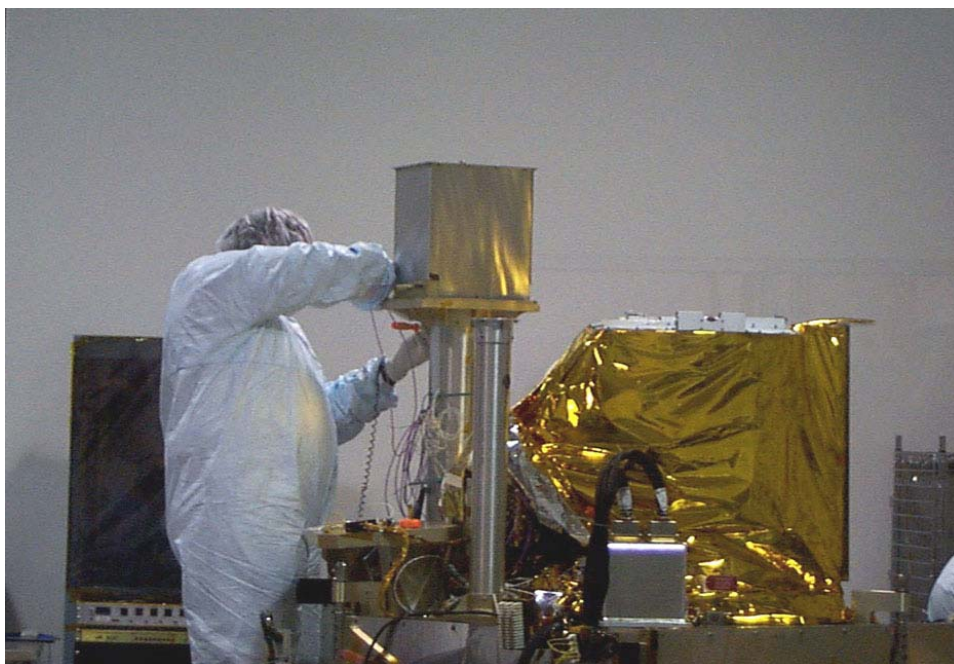


Figure 6. XPAA and test hood during integration with EO-1 spacecraft.

3. TECHNOLOGY VALIDATION

3.1 Brief Development and Flight History

In 1996, Boeing Defense and Space was selected to be a member of the NMP Communications Systems Integrated Product Development Team (IPDT) through a full and open competition for new technology managed by the Jet Propulsion Laboratory (JPL), with participation by the Lewis (now Glenn) Research Center (GRC) and GSFC. Promoting early flight of phased array technology on a NASA science spacecraft was a key objective identified by this IPDT.

Boeing proposed that it could build a phased array antenna for flight on the first NMP opportunity, the EO-1 mission. As a result, this technology was incorporated into the overall IPDT roadmap and earmarked for EO-1. The value of this technology was recognized in various NMP reviews, including those of the Architecture Design Team (ADT), and the Science Working Group (SWG). These reviews resulted in the Boeing X-band phased array, using the new acronym XPAA, being baselined for flight on EO-1.

A study contract was awarded to Boeing by JPL in the same year to address space flight qualification issues and to coordinate the loan of prototype RF modules and a 16-element engineering model antenna for evaluation at GRC. A sole-source fixed-price contract was negotiated and awarded by GSFC to Boeing on March 28, 1997, for one flight-qualified XPAA. The contract provided for a complete set of environmental acceptance tests to be performed, including thermal vacuum, vibration, and electromagnetic interference/electromagnetic compatibility (EMI/EMC).

Boeing delivered the XPAA to GSFC on October 9, 1998 at a formal Antenna Acceptance Review held in Seattle. GSFC turned over the antenna and acceptance data package to the EO-1 spacecraft integrator, Swales Aerospace, on October 22, 1998.

During the last week of November 1998, the antenna was moved to the laboratory clean room at Litton/Amecom in College Park, Maryland. It was connected to the EO-1 X-band exciter/modulator for the first time, and a compatibility test was run. During this test, 105-Mbps test data was sent through the X-band system and was received by the ground system receiver. Bit error rates (BERs) and other system operating parameters were measured.

Early in 1999, the antenna pattern of the XPAA was measured in the Swales Aerospace clean room using near field scanning equipment and expertise supplied by Near Field Systems, Inc (NSI). During this phase of testing a damaged MIL-STD-1773 fiber optic connector (one of four on the antenna) was found and replaced. The reliability of this connector was a global problem for EO-1 and other Goddard spacecraft. Numerous connectors used in other subsystems were also replaced.

In mid 1999, the antenna was brought to the EO-1 spacecraft where it was integrated with the rest of the system. After integration, environmental tests were conducted at the spacecraft level. After this, the effective radiated power, beam shape, and beam pointing capability of the XPAA were again verified while the EO-1 spacecraft was in GSFC's large clean room, the Spacecraft Systems Development and Integration Facility (SSDIF). Measurements were made with the same NSI near field scanning equipment used earlier.

EO-1 was launched from Vandenberg AFB in California in November 2000. Four days after launch, the XPAA was turned on for the first time. One orbit after turn on, data was successfully downlinked at 105 Mbps to the Spitzbergen, Norway, ground station. Soon after this, however, several ground stations reported that they were unable to reliably track and receive data from EO-1. The unreliable downlinks were reported at the Wallops, Alaska, and Norway 11-meter stations, all of which required X-band auto track systems to

maintain antenna pointing. The fact that several stations seemed to have the same problem, and only with EO-1, appeared to indicate a problem on the spacecraft, perhaps with the XPAA.

At the request of NMP management, a tiger team was formed with members from Boeing, GSFC, GRC, and JPL. The collective experience of the members covered the XPAA itself, phased arrays in general, NASA ground networks and tracking systems, and the specific ground stations involved. Attempts to characterize the problem by gathering and contrasting specific attributes of successful and unsuccessful downlinks continued through December and into January.

Because the three ground stations involved used nearly identical hardware, other stations with different equipment were requested to attempt downlinks. As the data was assembled by the tiger team, it gradually became clear that ONLY the original three stations were experiencing real problems with tracking the EO-1 emission.

The health of the XPAA was evaluated by performing several elements of the original validation plan, including observing the downlink spectrum, estimating the antenna's EIRP, comparing the variation in EIRP with predictions, and capturing an antenna pattern from orbit. The results of these measurements revealed no detectible problem with the performance of the XPAA.

Ultimately the problem was traced to different hardware problems at each of the three ground stations that only manifested themselves when they were configured for left-hand circular (LHC) polarization. As was stated earlier, EO-1 was the only LHC spacecraft to be tracked by these antennas. Once these problems were identified and corrected in February 2001, the stations performed reliably, providing error-free downlinks. Since that time, the XPAA has been used five times per day on average for more than one year, far exceeding the design requirement of once per day, with 100% reliability.

3.2 Validation Overview and Results

The validation plan for the XPAA called for collecting data to meet the following objectives:

1. Validate the communications link error performance. Phased arrays are unique in that they cause phase disturbances in the emitted signal whenever the beam position is changed. This disturbance has the potential to cause errors in received data, and can be corrected by appropriate error correction coding of the data. This objective will also validate whether the error correction coding used by NMP/EO-1 is adequate for the task of correcting phased array induced errors as well as those caused by atmospheric, RF interference, and other traditional sources.
2. Validate the antenna pattern scan performance of the phased array. Phased arrays are unique in that the antenna gain and EIRP change with pointing angle. It must be shown that this performance can be reliably predicted and maintained during the life of a mission.
3. Validate the performance and reliability of the antenna's electronics and software in the space environment. Besides validation of the functions themselves, this information is necessary in assuring that RF performance issues which may be attributed to the transmit elements are not actually errors due to incorrect operation or programming of the controller.

The following sections document the results obtained from the validation activity.

3.3 EO-1 XPAA Link Error Performance

3.3.1 Introduction

EO-1 downlinks to 11.3-meter dishes in Poker Flats, Alaska; Svalbard, Norway; and Hobart, Australia, have over 10 dB of margin and are virtually error-free over 10-minute passes. The upper limit to the BER is consequently 1.6×10^{-11} . To search for errors induced by beam steering and to test the coding, the signal had to be degraded. Validation tests were performed with the 3-meter Goddard Ground Station (GGS) antenna at Bldg. 28 at GSFC. Variable amounts of noise were added to the signal received to degrade link performance. No effects from the beam steering phase disturbances are detected. The coding on the link is shown to be adequate. Full descriptions of the XPAA and validation tests follow below.

3.3.2 Phased Array Antenna Characteristics

The XPAA was designed and built by Boeing's Phantom Works in Seattle, Washington. It consists of an 8-by-8 array of radiating elements, each fed through a circular waveguide by dual power amplifiers operating 90° out of phase to create LHC polarization. The antenna and control electronics fit into a 12-inch x 13-inch x 2.9-inch enclosure. The EO-1 XPAA operates at 8225 MHz with a 22-dBW minimum EIRP. The 64 radiating elements are each phased by a 16-step (4-bit) phase shifter to shape the beam. The beam can be steered to 60° from normal with the EIRP decreasing as cosine of the zenith angle.

Operationally, when the beam is steered as EO-1 passes over the ground station, the in-phase pairs of elements are changed to keep the phase center of the antenna at the center of the array. So one edge element may advance in phase by 22.5° and the element opposite it will recede by 22.5° . At the maximum tracking rate on orbit, generally no more than 4 elements need to be switched at once, except in rare cases when up to 16 elements may be switched. The phase noise associated with this switching ($\pm 0.3^\circ$) is less than the phase noise of the system and is not expected to affect the BER.

The phase information is passed to the element modules at 2 Hz. The EO-1 X-band data rate is 105 Mbps for a dual data channel. So there is 52.5 Mbps on both the I and Q channels. A search for errors occurring at 2 Hz (26.25 Mbits) investigates the effect of beam steering on the BER.

3.3.3 Link Characteristics

The EO-1 data is Reed-Solomon coded, randomized, and differentially coded onto the I and Q channels before quadrature phase shift key (QPSK) modulation on the 8225 MHz carrier. Error correction is provided by the Reed-Solomon (252,220) code with an interleave depth of $I=5$. The Consultative Committee for Space Data Systems (CCSDS) virtual channel data unit (VCDU) is $252 \times 5=1260$ bytes. Randomization is applied to the VCDU according to CCSDS 101.0-B-4 to ensure ground receiver acquisition and sufficient bit transition density for the bit sync to maintain lock. The randomized VCDU is then appended to a 4-byte attached sync marker (ASM) to form a 1264-byte CCSDS channel access data unit (CADU).

The QPSK link is configured as a dual data channel, so the I and Q channels each have their own stream of CADUs. A quadrature differential (Gray) code converts a pair of bits from the two input channels to I and Q bits on the link. The code is an analog to the NRZ-M format for a single channel. The quadrature differential code resolves channel and phase ambiguity when the signal is received on the ground. Like the conversion from non-return to zero (NRZ)-M to NRZ-L, the decoding process gives two consecutive errors in the decoded stream for a single error in the transmitted signal. The details of the differential coding are included in Appendix A.

The quadrature differential code determines how the data are phase shift keyed (PSK) onto the carrier. QPSK uses phase shifts of 90° and multiples thereof to represent bits and is the most power efficient method of data modulation. However, when PSK modulation is used with a phased array antenna, the additional phase shifts

associated with steering the beam may interfere with the phase shifts of the data bits. Since the phase shifts associated with steering the beam ($\sim 0.3^\circ$) are small compared to those due to data bits (90°), the effect is expected to be small.

3.3.4 Test Procedures

Weekly downlinks to GSFC were scheduled to support this validation effort. During a typical 10 minute EO-1 pass over the GSFC ground station, one or two data sets of gigabyte size are recorded on an AMPEX tape player. From May 2001 to October 2001, over 17 Gbytes of data were recorded and analyzed with custom software to determine the EO-1 XPAA bit error performance.

3.3.5 Data Collection

The EO-1 XPAA downlink is received at the GSFC ground station with a 3-meter antenna. Since the link has adequate margin for a burst error rate (BER) of 10^{-7} , we adjust the background noise level into the receiver to simulate conditions of degraded link margin. Adding noise yields BERs over two orders of magnitude, from 10^{-5} to 5×10^{-3} . We record data on AMPEX tape in files of up to 2 minutes (about 1.5 Gbytes).

The GSFC ground station is reconfigured as in Figure 7 to add noise to the received signal. A Noise/Com Precision Carrier-to-Noise (C/N) Generator (UFX-BER Series) operates at an intermediate frequency (IF) of 720 MHz. Mini-Circuits mixers (ZLW-2) up-convert the 375 MHz IF signal from the ground station to 720 MHz and down-convert the Noise/Com output back to 375 MHz. A Mini-Circuits 850-MHz low pass filter rejects the 1095 MHz local oscillator (LO) and upper sideband before the Noise/Com input. The Radarsat receiver operates at 375 MHz.

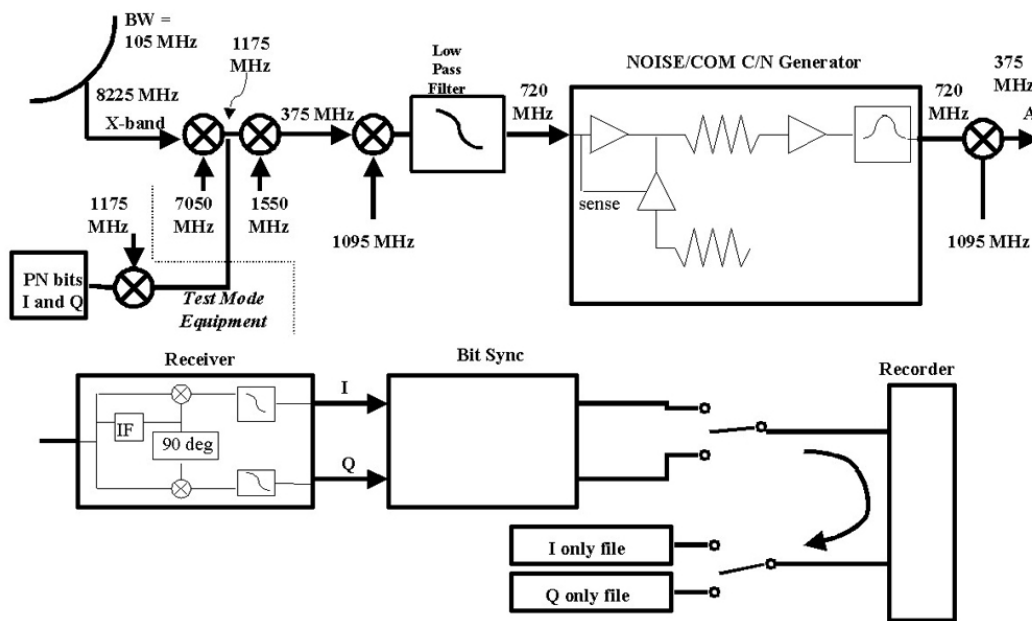


Figure 7. Ground station configuration.

The EO-1 XPAA turns 90 seconds after reaching 5° -elevation angle. It starts with a fill pattern for 30 seconds and then sends science data. During the initial acquisition, the Noise/Com is set in “Meter” mode, with the signal passing straight through with no modification. After signal acquisition in the demodulator and bit sync, the Noise/Com is manually set in “C/N” mode with the parameters in Table 1.

Table 1. Noise Injection Parameters

Parameter	Symbol	Value
Carrier Level	C	-15 dBm or -22 dBm
Signal Bandwidth	Sbw	100 MHz
Noise Bandwidth	Nbw	648 MHz
Carrier Frequency	CF	720 MHz
Carrier to Noise Ratio	C/N	various (5-20 dB)

The Noise/Com requires an input signal greater than C to operate. The output signal level will initially be C but will vary thereafter with the input signal level. Upon manually starting the noise generator, the output signal is interrupted. Once the receiver and bit sync reacquire, data is recorded on the AMPEX tape. Short (1-2 Gbytes) files are recorded for ease of data analysis.

3.3.6 Data Analysis

A combination of existing and new software is used to analyze the recorded EO-1 downlink stream. The first set of programs reverses randomization and coding processes performed by the EO-1 spacecraft. Comparison of the input and output of the decoding process determines the location of errors in the downlink. The next program calculates the burst error statistics and periodicity. These data are displayed and a test is performed to determine whether the XPAA beam steering degrades the link performance.

Files of the bits received on the I channel and the Q channel are separately extracted from the AMPEX tape. These files contain the continuous stream of bits after the differential decoding process. The steps to determine where bit errors occur are performed independently on the two channels. We search a raw data file for the ASM in a channel and byte-align the output with the ASM. Only data between two valid ASMs is output, however the software allows for up to 5 bit errors (selectable) in the 32-bit ASM. To maintain the timing and synchronization between the two channels, the bit location in the input file of the beginning and end of all output data is recorded.

Next, the randomization process is reversed and decoding is done. Derandomization is performed by a modulo-two addition of the same pseudo-random noise (PN) pattern used to randomize to the VCDU. In the decoding process, correctable errors are fixed but uncorrectable frames are left as is. Reed-Solomon statistics, like the number of correctable and uncorrectable frames, the total number of code blocks, number of uncorrectable and correctable code blocks and correctable bit errors, are output. From these the overall BER is determined as

$$BER = N_e / \{252 * 8 * (B_t - B_u)\},$$

where N_e is the number of correctable bit errors, B_t is the total number of codeblocks, B_u is the number of uncorrectable code blocks, and $252 * 8$ is the number of bits per codeblock. Since this estimate excludes frames with too many errors to correct, it slightly underestimates the actual BER.

The program “errcomp” compares the data pre- and post-decoding to determine the locations of the correctable errors. Since there are relatively few errors, the number of bits between consecutive errors is stored in lieu of storing a copy of all the bits.

After the locations of errors are known for both channels, the two records are combined to determine the location of all errors. The error locations come from data byte-aligned to the channel ASM, which are not synchronous between the two channels. A record of the bit position of the starting ASM, generated in the frame sync process, is used to align the two channels.

This combination occurs during the program “phasehist” which bins the errors by their location in the 0.5 sec beam-steering period. Errors that occur at random intervals will have an equal probability of filling any bin.

Errors that occur with a 0.5 sec period or any multiple of 0.5 sec will fill just one bin. Since there are 26,250,000 bit periods every 0.5 seconds, we use 26,250 bins that are 1000 bits wide. This makes a reasonable number of bins and also allows for timing differences in the switching and data systems. “Phasehist” outputs the total number of errors occurring in each bin.

To test whether the phase shifts occurring because of steering the beam affect the PSK of the data bits, we run “phaseshift” twice for each data set. The first time, we use bins that are 1000 bits wide as described above. Then second time is a control used for comparison. It has bins 887 bits wide. Errors that occur every 0.4435 seconds would show up in one bin for this run. The results of the second run are used as a baseline for a set of errors for which no repetitive signal is expected.

While the two sets of error locations are read in by “phasehist,” burst error statistics are calculated. A burst is defined as a single error or a set of errors about which a minimum number of correctly transmitted bits occur in both channels. For this test, 50 correctly transmitted bits occur before and after each burst. The number of errors and length of each burst is recorded. The length is defined as the distance between the first and last error of the burst. Since the EO-1 link is a differentially coded QPSK link, a single transmitted error can cause a single error in both the I and Q output data. Within this definition of a burst, an error at bit position p in channel I would be in the same burst as an error at bit position $p + 15$ in channel Q, for example.

Armed with the burst statistics and the number of errors in 26,250 intervals within the ½ second beam steering period at various BERs, we can characterize the EO-1 link bit error performance.

3.3.7 Results

This report summarizes over 13 Gbytes ($>10^{11}$ bits) of the EO-1 XPAA data collected and analyzed as described above. Table 2 shows the size of the files collected and an estimate of the BER. It should be used as the key to the graphs below to identify the curves with an actual BER. The actual estimated BERs span two orders of magnitude, from 10^{-7} to 7×10^{-3} , which is close to the limit of the Reed-Solomon code’s ability to correct random errors.

Table 2. BER Data Sets

BER#	Date	BER	Size (bytes) (single channel)	Number of 0.5-sec. periods
1	19 Jun 2001	1e-5	558225400	85
2	13 Sep 2001	5e-5	705333488	107
3	13 Sep 2001	6e-5	1350836224	205
4	21 Sep 2001	1e-4	881342328	134
5	21 Sep 2001	2e-3	891876504	135
6	9 Aug 2001	5e-3	816258336	124
7	21 Sep 2001	7e-3	555343456	84
CTL	17 Oct 2001	1e-7	756621552	115

3.3.8 Burst Error Statistics

The burst error statistics for the 5 data sets are plotted in Figure 8. For each data set with $BER < 3 \cdot 10^{-3}$, there are more bursts with 2 errors per burst than any other number of bursts. Two is also the most common length of a burst. Differential decoding leads to two errors in the data bits for a single error in the transmitted bits. So the burst statistics show that on the physical link, single bit errors are most common.

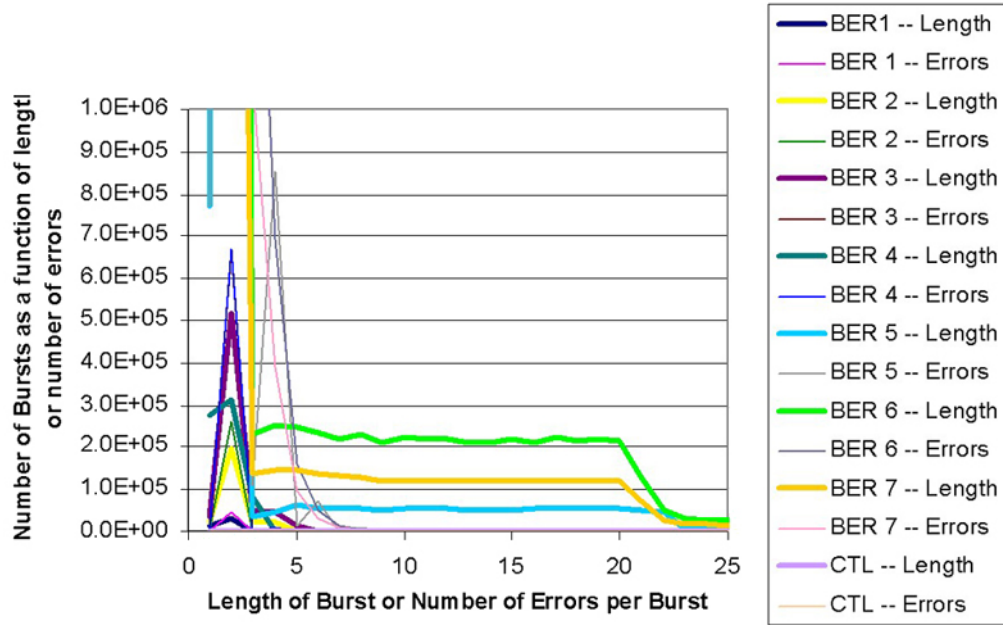


Figure 8. XPAA burst error statistics.

The curves in Figure 8 are not normalized to the BERs. BER 6 has more bursts than BER 7 because it is a larger file despite having a lower BER. The data sets with BER greater than 10^{-3} have a significant number of bursts with lengths between 5 bits and 25 bits. They have bursts with lengths greater than 50 bits that do not appear on the graph. These bursts mostly have just a few errors and none have more than 20 errors per burst.

3.3.9 Periodic Errors

To determine if the 0.5-second phase shift period for beam steering affected the bit error performance of the XPAA, we binned the errors according to their location in the period. Figures 9 through 13 show plots of the number of errors in the 26,250 bins 1000 bits wide of a 0.5-second period. All the graphs show that the number of errors in any bin is randomly distributed about an average value consistent with the overall BER. If steering the beam causes an error every 0.5 second, one bit of the 26,250 would have many more errors than any other. We see no evidence of any effect of beam switching on the bit error performance.

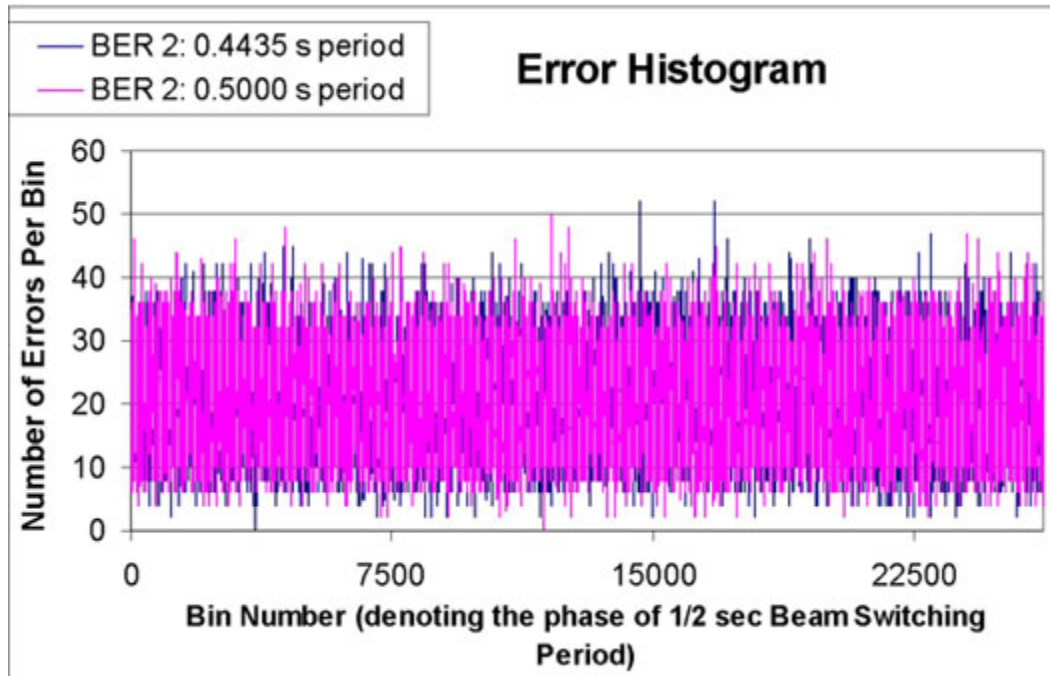


Figure 9. Error histogram (1).

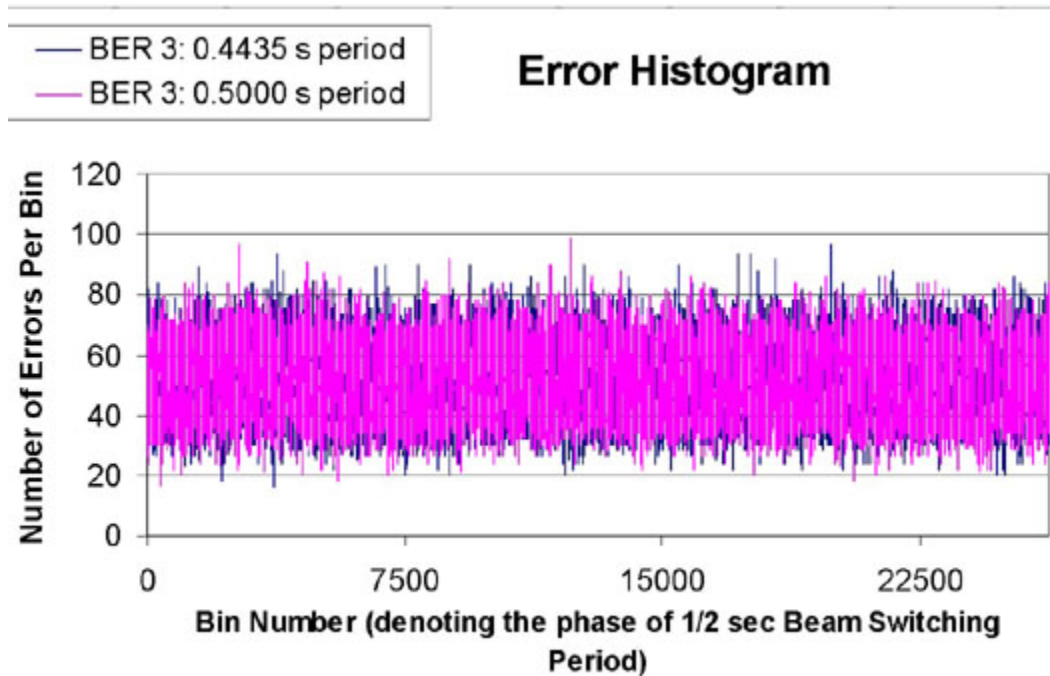


Figure 10. Error histogram (2).

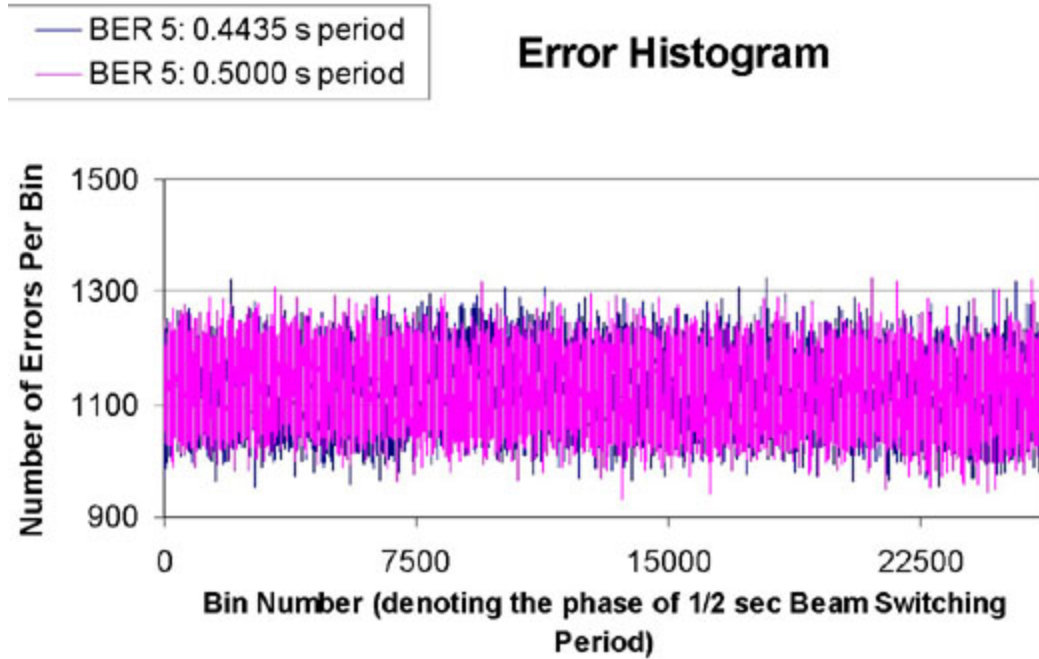


Figure 11. Error histogram (3).

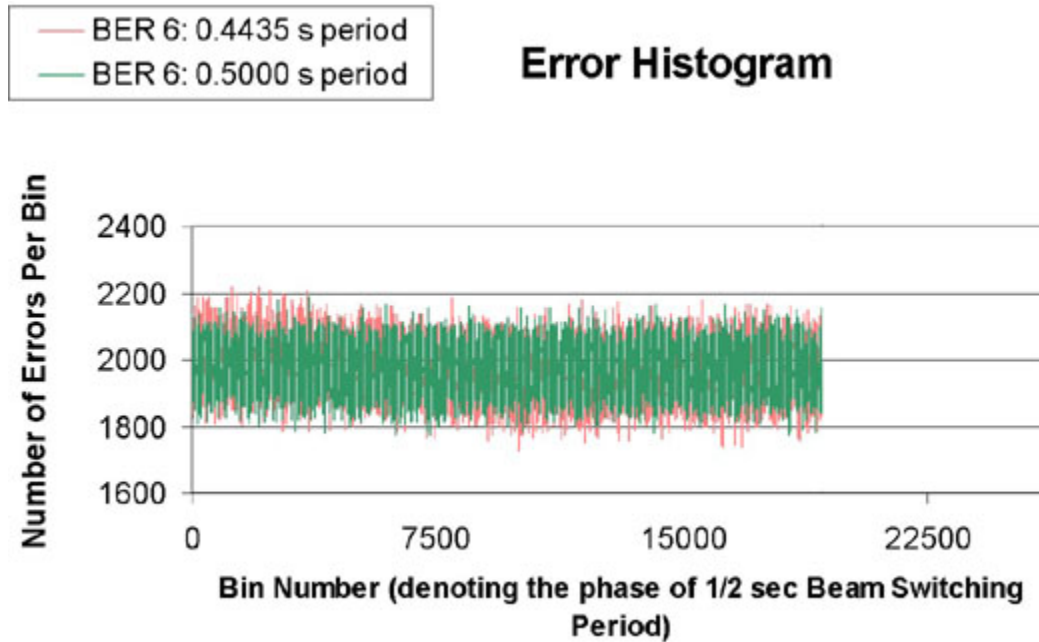


Figure 12. Error histogram (4).

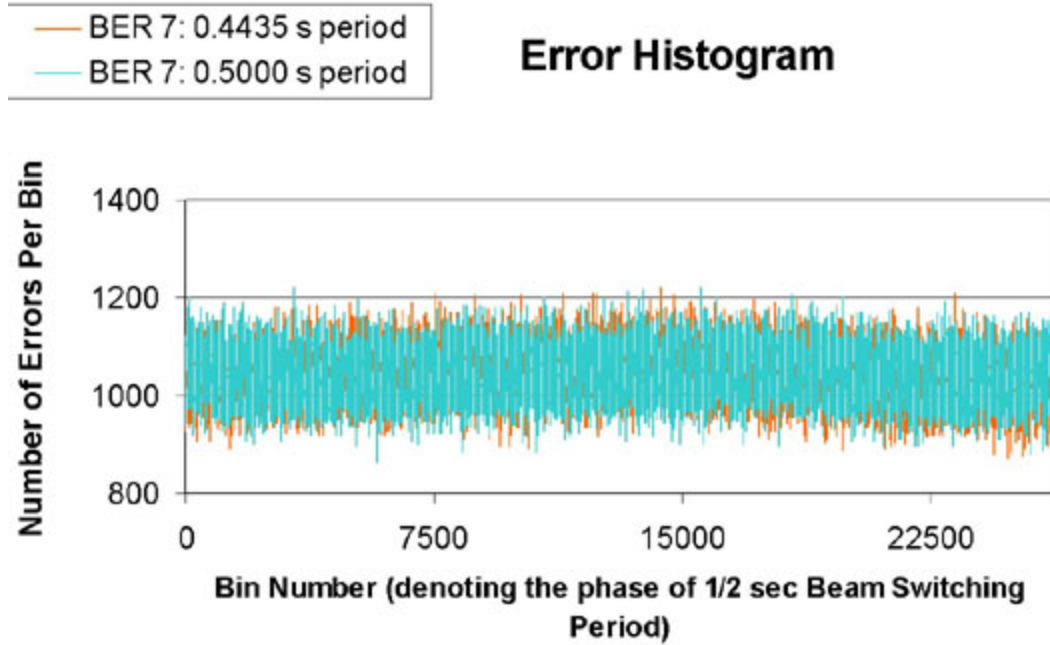


Figure 13. Error histogram (5).

It is useful to compare the results among the various BERs. At low BERs, we have a strong signal and do not expect the beam steering to interfere with the phase shift keying of the bits. At the higher BERs, when we injected noise before the receiver, the noise added to the phase shifts associated with beam steering may be more likely to cause bit errors. If an error occurred every 0.5 second due to beam steering, we can calculate the number of errors due to beam steering. It is equal to twice (because of quadrature differential coding) the number of 0.5 seconds of data collected (in column 5 of Table 2). In BERs 2 and 3, having 200 and 400 errors in one bin would stand out as obvious. But for BERs 6 and 7, an additional 240 and 170 errors per bin is within the noise in the number of errors per bin.

Table 3 contains a summary of the statistics of the number of errors per bin when binned for the 0.5-second beam steering period. It lists the total number of bit errors in each data set, the average number of errors in one bin, the standard deviation of the number of errors per bin, and the minimum and maximum number of errors in a bin. The final row indicates the variance (σ^2) in the number of errors per bin decreases with the total number of errors, as one would expect for random data. Table 3 shows that 240 and 170 additional errors per bin for BERs 6 and 7 are at least 4σ , they are smaller than the overall peak-to-peak variation of the errors per bin.

Table 3. Error Histogram Statistics

BER	1	2	3	4	5	6	7	CTL
N, Tot Errors	87542	527551	1344651	1380105	29595984	51798226	27415949	1856
Avg (μ)	3.335	20.097	51.225	52.575	1127.466	1973.266	1044.417	0.071
Std. Dev. (σ)	2.587	6.339	10.043	10.369	48.186	56.973	44.322	0.324
Min	0	0	17	16	930	1767	863	0
Max	20	50	99	99	1324	2192	1221	4
$\sigma/\mu*\sqrt{N}$	229.5	229.1	227.3	231.7	232.5	207.8	222.2	196.6

For this reason, the 0.4435-second histogram is plotted in Figures 9 through 13 behind the 0.5000-second histogram. Visually, the statistics of the two histograms looks the same in every case. The actual distributions

of errors per bin were studied to reveal no significant difference in the two periods. Figures 14 to 16 show these distributions. In Figure 14, the low BERs are shown: the CTL data set is compared to a Poisson distribution and BERs 2 and 3 are compared to Gaussian. The agreement is moderate for the small number of errors per bin. In Figures 15 and 16, the distributions for BERs 5, 6 and 7 are compared to Gaussians and the fit good. Even though there are some bins with over 200 more errors per bin than the average (an expected signal level for an error every 0.5 second), given Gaussian statistics we expect to see as many as we do. These distributions and the original graphs of errors per bin (Figures 9 through 13) show no sign of periodic errors caused by beam steering.

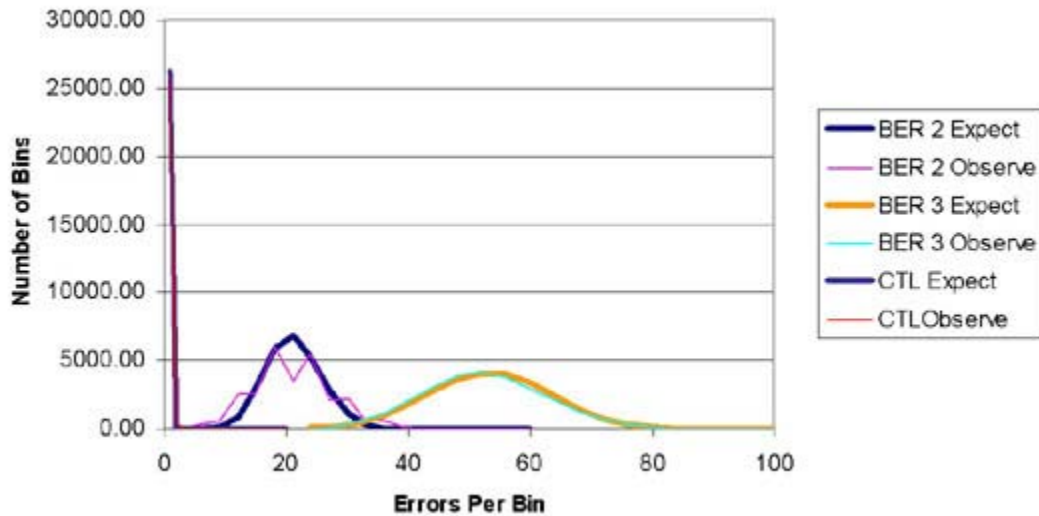


Figure 14. Errors per bin distribution (1).

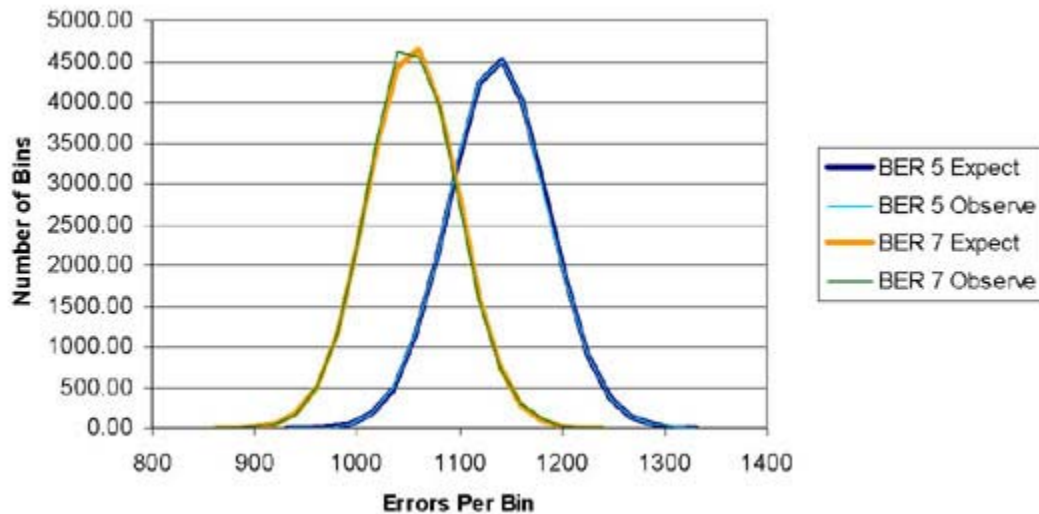


Figure 15. Errors per bin distribution (2).

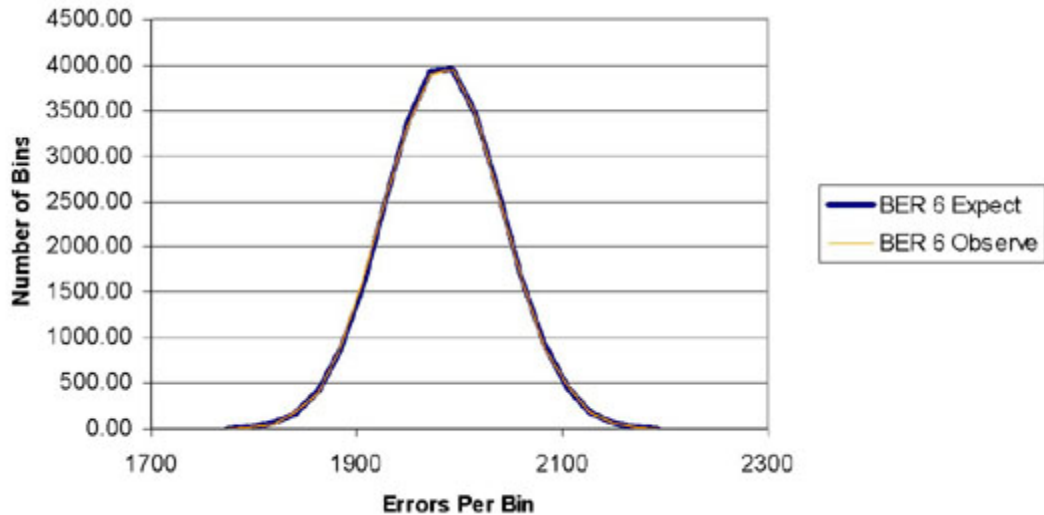


Figure 16. Errors per bin distribution (3).

3.3.10 Conclusion

The EO-1 XPAA validation of bit error performance found no evidence of bit errors inherent to the XPAA. Burst error statistics were consistent with the differential coding performed on the spacecraft. Data collected with various background noise levels indicated that phase shifts associated with steering the beams on the phased array do not interfere with the phase shift keying of data bits on the link. The Reed-Solomon and differential coding was adequate to correct errors within the power of the Reed-Solomon code.

3.4 EO-1 XPAA Antenna Pattern/Scan Performance

3.4.1 Introduction

This section summarizes the verification of the antenna pattern scan performance of the phased array, from acceptance testing done at the Boeing plant, through integration and test (I&T) at GSFC, ending with measurements conducted from ground stations after EO-1 was launched.

3.4.2 Anechoic Chamber Patterns and Near Field Scans Prior To Launch

Before and after delivery by Boeing to GSFC, the phased array radiation patterns were measured by the planar near field technique. The planar near field technique consists of measurement of the amplitude and phase of the radiated field several wavelengths in front of the antenna aperture. Far field patterns are then calculated from this data.

Prior to delivery to GSFC, Boeing conducted numerous acceptance tests on the XPAA, including shock, vibration, EMI/EMC, and thermal vacuum. Between each test, the health of the antenna was evaluated using either a Comprehensive Performance Test (CPT) or a Limited Performance Test (LPT). CPTs of the XPAA included a set of antenna patterns taken in an anechoic chamber facility and were used as the basis for the Government's acceptance of the antenna. LPTs, as the name implies, were a more limited, but faster series of tests run between environmental test phases to prove that the antenna was still working properly. Near field scans were taken instead of traditional antenna patterns during LPTs.

After delivery to GSFC, there were a number of RF tests performed on the X-Band Array before and during the EO-1 spacecraft integration. The tests confirmed the radiation pattern beamwidth and sidelobe levels and verified commanded scan positions. Repeated near-field measurements during these phases were shown to be

a good diagnostic tool for discovering any antenna performance degradation caused by post-delivery handling, spacecraft vibration and thermal-vacuum tests, or other anomalies. Near-field data processing software also generated holograms that allowed insight into the array aperture amplitude and phase distribution. Figures 17 and 18 are photographs of the near field scanner test setups at Swales Aerospace prior to delivery to GSFC and at GSFC after spacecraft integration, respectively.

The EIRP of the array was measured using a comparative near field technique. This method consists of measurement of a gain standard horn antenna using the planar near field scanner and then the phased array is measured. The EIRP of the array is then determined from the comparative measurement with the gain standard horn antenna. The phased array can then be scanned in angle and the EIRP measured versus array scan position. The array maximum EIRP measured 57.0 dBm +/- 2 dB as the average of five different measurements based upon a method developed by the National Institute of Standards and Technology as described in reference 2.



Figure 17. Post-delivery tests of the XPAA using the NSI near field scanner at Swales Aerospace.

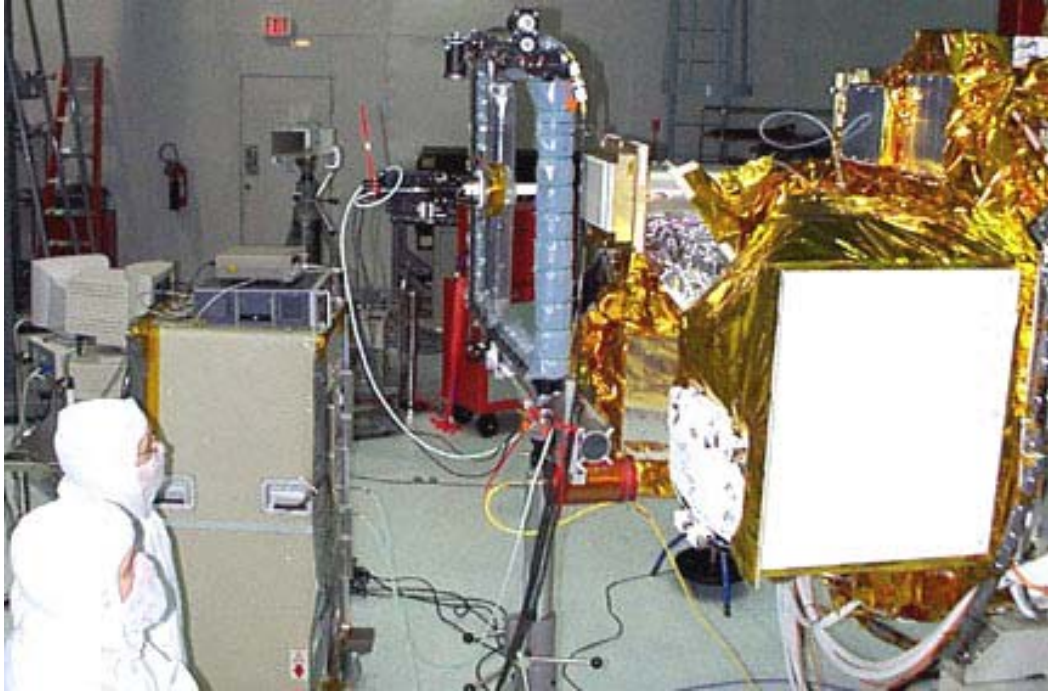


Figure 18. Near field scanning the XPAA after integration with EO-1 at GSFC. This setup was also used for the final EIRP measurement before EO-1 was shipped to the launch site.

3.4.3 Integration and Test Results

Near field measurements of the XPAA after delivery to GSFC were compared to those obtained with Boeing's anechoic chamber measurements. Figure 19 shows the near field result overlaid on the anechoic chamber pattern for the case when the XPAA's beam is pointed to $\theta=0$ degrees, $\phi=0$ degrees (boresight). Figure 20, similarly, shows the result for $\theta = 45$ degrees, $\phi = 0$ degrees. On both of these plots the near field pattern, in red, is offset so that both patterns can be seen clearly. Very good correspondence is seen in the relative sidelobe levels and the location of the nulls between them.

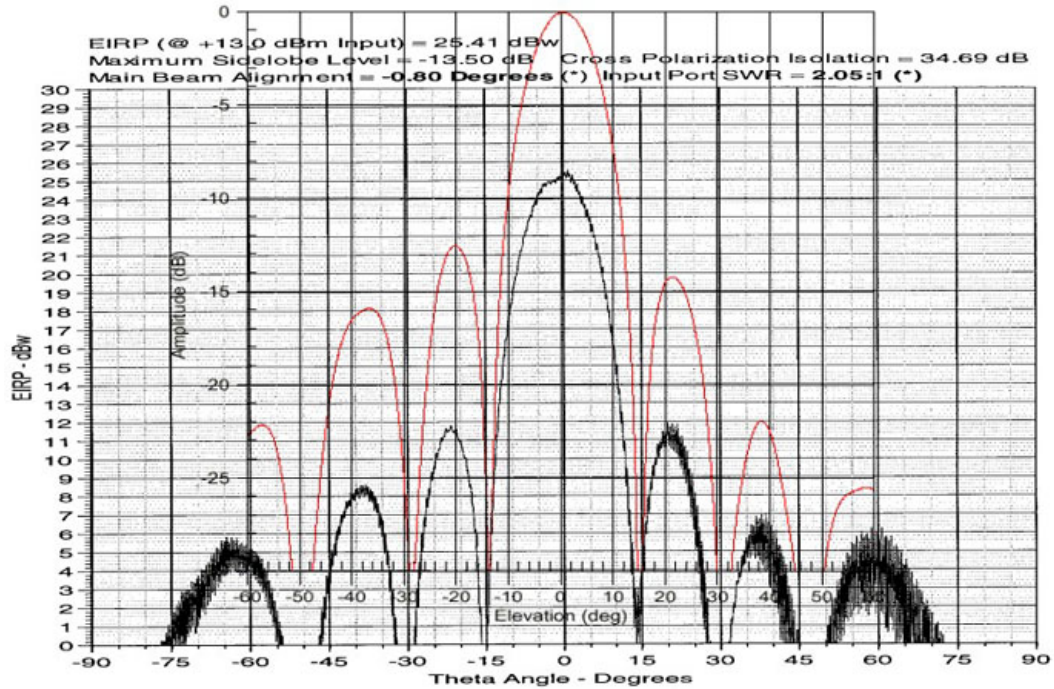


Figure 19. Comparison of pattern calculated using NF data taken at GSFC (red) with the equivalent Boeing anechoic chamber pattern ($\theta = 0, \phi = 0$).

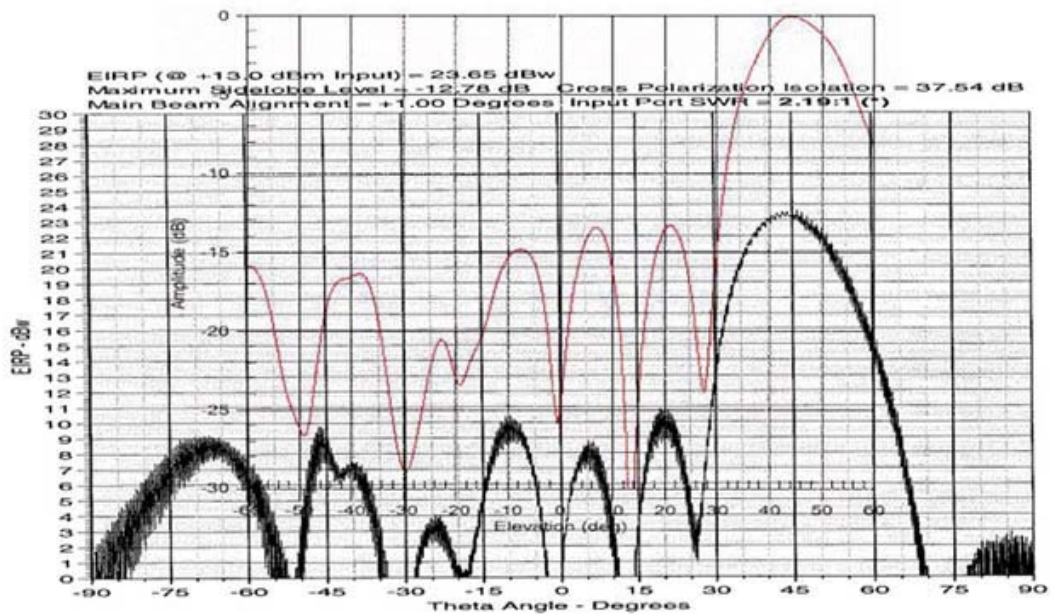


Figure 20. Comparison of pattern calculated using NF data taken at GSFC (red) with the equivalent Boeing anechoic chamber pattern ($\theta = 45, \phi = 0$).

The near field measurements provided a trending data set that traced the antenna pattern performance of the XPAA from factory through integration and test, up to shipment of the EO-1 spacecraft to the launch site. Figure 21 displays three sets of near field data as two-dimensional contour plots. Left to right, they depict the XPAA's pattern as measured at Boeing's plant, at Swales prior to integration with EO-1, and after integration.

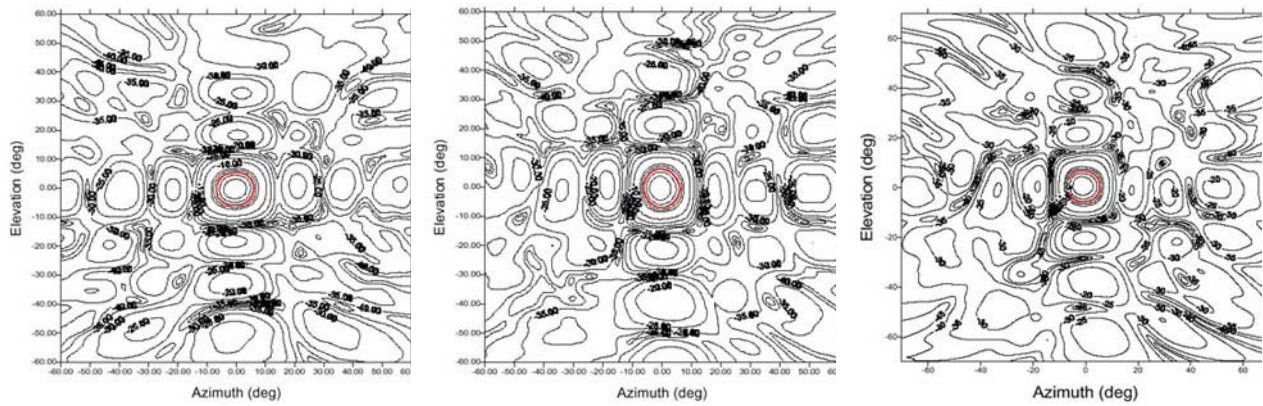


Figure 21. Calculated XPAA contour plots from near field measurements taken at Boeing prior to delivery, at Swales before integration with EO-1, and after integration.

The NSI near field scanning software also provided an ability to generate holograms depicting the amplitude and phase of RF energy at the antenna's aperture plane. Viewing the trending data in this format enabled insight into changes in the health or functioning of the individual array elements. Figure 22 shows a set of this data taken prior to integration with the spacecraft. Data taken from before delivery and after integration was similar, revealing no significant changes over time. The holograms indicated that all 64 transmitting elements of the array were operating properly throughout EO-1's ground testing.

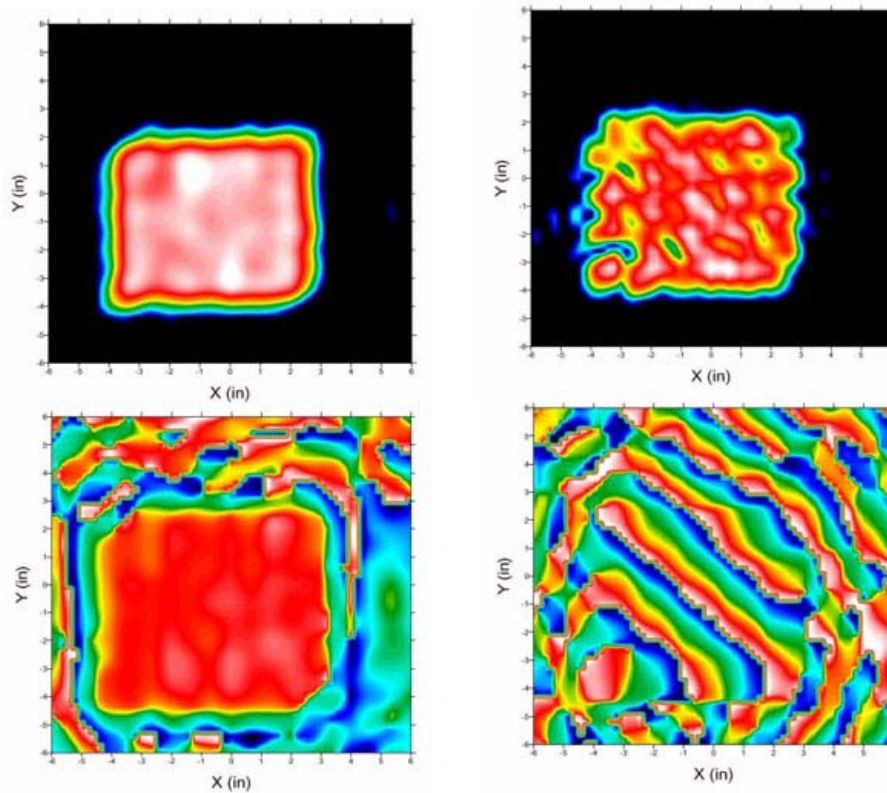


Figure 22. Near field data showing the calculated amplitude (top) and phase (bottom) distributions across the aperture of the XPAA when pointed to $\theta=0$, $\phi=0$ (left) and $\theta=45$, $\phi=315$ (right).

3.4.4 On-Orbit Tests Using Ground Stations

After EO-1 had achieved orbit and begun science operations, the performance of the XPAA was validated, first and foremost, by the conduct of successful science downlinks. These were routinely achieved within the first two months of the mission, after initial problems with ground station configurations were identified and resolved as described earlier. The XPAA's antenna pattern and performance, while scanning, were also measured from the ground and compared with pre-launch data.

During each of these tests, EO-1 transmitted 105-Mbps science data via the XPAA. At the ground sites, received signal strength and signal-to-noise ratio were measured by recording the downlink spectrum using a spectrum analyzer. Specifically, to accomplish the spectrum recording, an HP8566 spectrum analyzer was connected to the IF output from the ground station antenna's low-noise amplifier (LNA)/downconverter, which could be expected to provide a linear response. The resultant spectrum was recorded at a rate of 2 traces/second from the analyzer via its general purpose interface bus (GPIB) interface with a laptop computer using the software program called "Specviewer." A companion program "Specdata" was used to integrate the power across a 100-MHz bandwidth and record the result versus Global Positioning System (GPS) time. This arrangement provided much finer resolution of variations in received power than was normally available using the automatic gain control (AGC) data from the ground stations. The Specdata results were then transferred to an Excel spreadsheet where they were corrected for calculated range loss. Examples of these results are shown in Figure 23. This data was merged with time-tagged aspect angle data from EO-1's attitude control system, to calculate emitted power versus aspect angle.

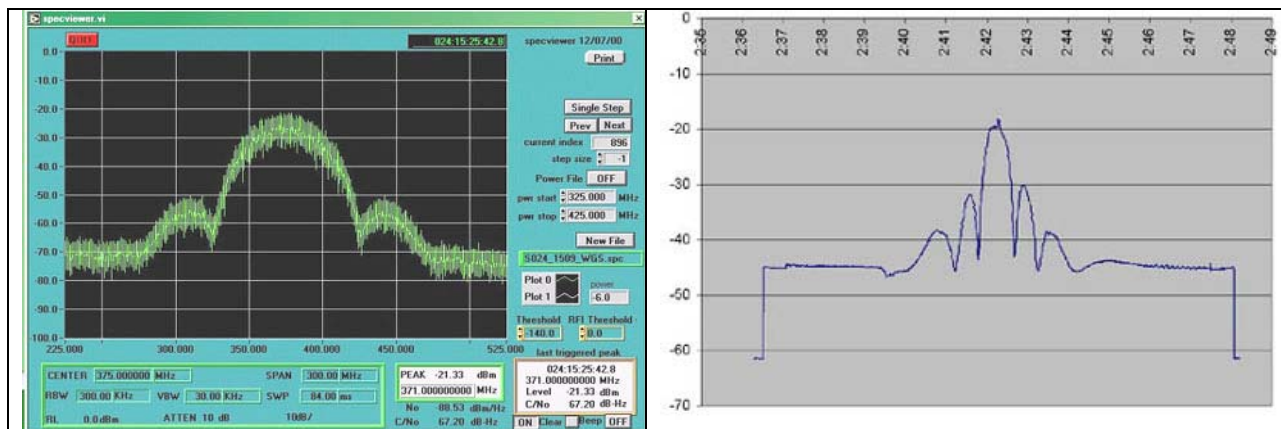


Figure 23. Example of EO-1's X-band frequency-domain spectrum that was recorded with the "Specviewer" program (left) and the resultant time-domain Excel plot of XPAA emitted power from "Specdata" corrected for range variations during the pass (right). The XPAA was pointed to boresight throughout the pass.

3.4.5 Antenna Pattern Results

For antenna pattern measurement, the XPAA was set to point its beam to boresight (elevation angle $\theta=0$, azimuth angle $\phi=0$) during a near-overhead pass to the ground station. As EO-1 passed over the ground station, the received power on the ground would vary with range and the XPAA antenna pattern as the aspect angle with EO-1 changed. Because the received power would vary greatly during this measurement, a ground station capable of open loop "program tracking" by computer was required. The GSFC three-meter antenna at Building 28 was used for this purpose.

Figure 24 depicts the traverse of the ground station position through the XPAA's boresight pattern during one such overhead pass. The path of the pattern cut is a curve that cuts within 5 degrees of the peak of the main

beam. Figure 25 shows the resulting pattern that was produced, in black squares. The red diamond data that is overlaid is the equivalent curved cut obtained from near field scans prior to launch. The gap in the center results from the fact that the cut does not cross the peak of the beam. The deviation of the measured data near the peak of the main beam is attributed to dynamic errors in ground station antenna pointing, which are worst when the satellite is at maximum elevation.

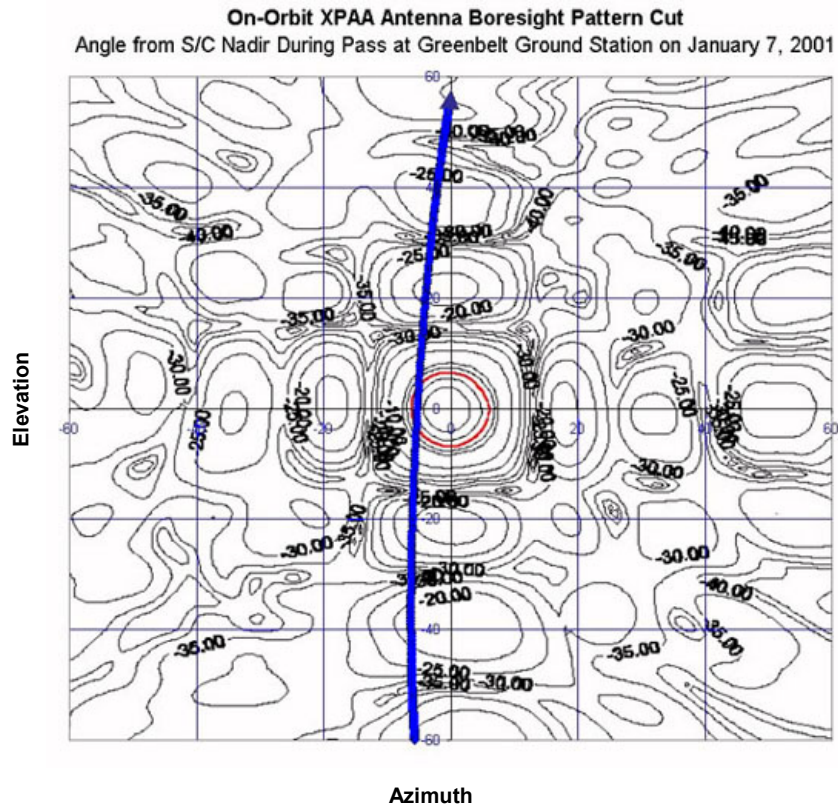


Figure 24. Antenna pattern cut taken from orbit as EO-1 passed over GSFC. Angles are shown in degrees (large divisions = 20 degrees).

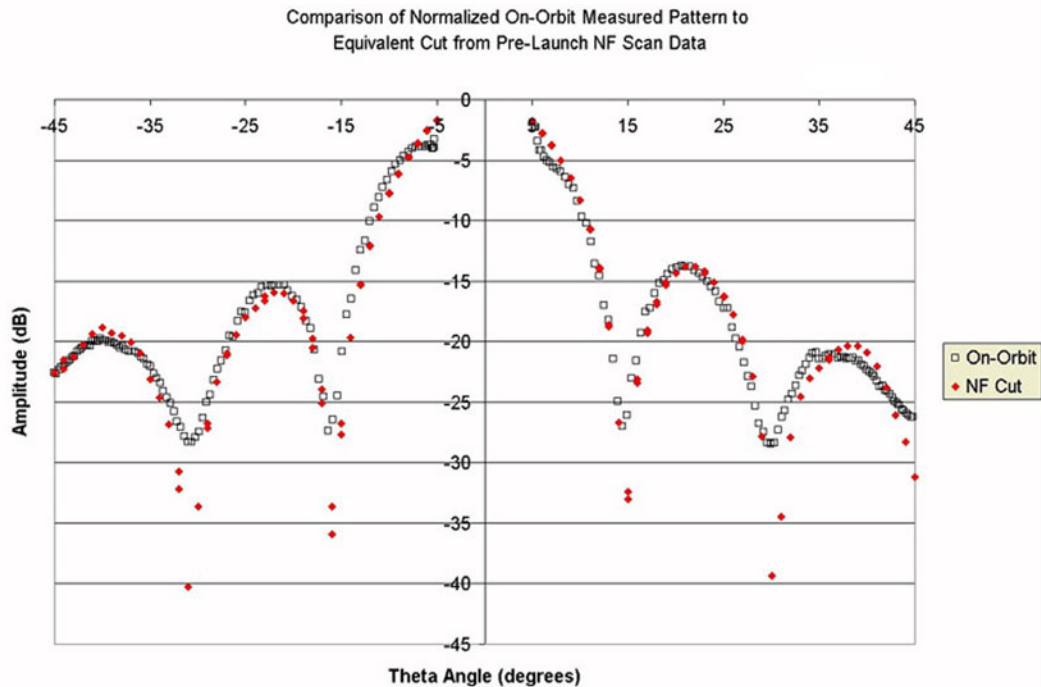


Figure 25. Antenna pattern from EO-1 after launch, adjusted for range and path losses, compared to equivalent cut derived from pre-launch near field measurement data.

3.4.6 Scan Performance Results

For scan-performance measurement, the XPAA was operated normally; its beam pointed every half-second toward the ground station by commands from EO-1’s attitude control system. As EO-1 passed over the ground station, received power varied as the EIRP from the XPAA changed due to range and scan angle effects. The 11-meter antenna at Wallops Flight Facility was used to collect this data, usually in conjunction with a normal instrument data downlink. These measurements were made on clear days when rain attenuation was not a factor.

Figure 26 depicts the results from one such test of the XPAA. Curves showing the elevation of EO-1 as seen from the ground during the pass, and the EIRP expected from XPAA, and published characteristics for the Wallops ground station were used in calculating the predicted signal-to-noise ratio. The signal-to-noise ratios calculated from the Specviewer data show surprisingly good agreement with the measured values.

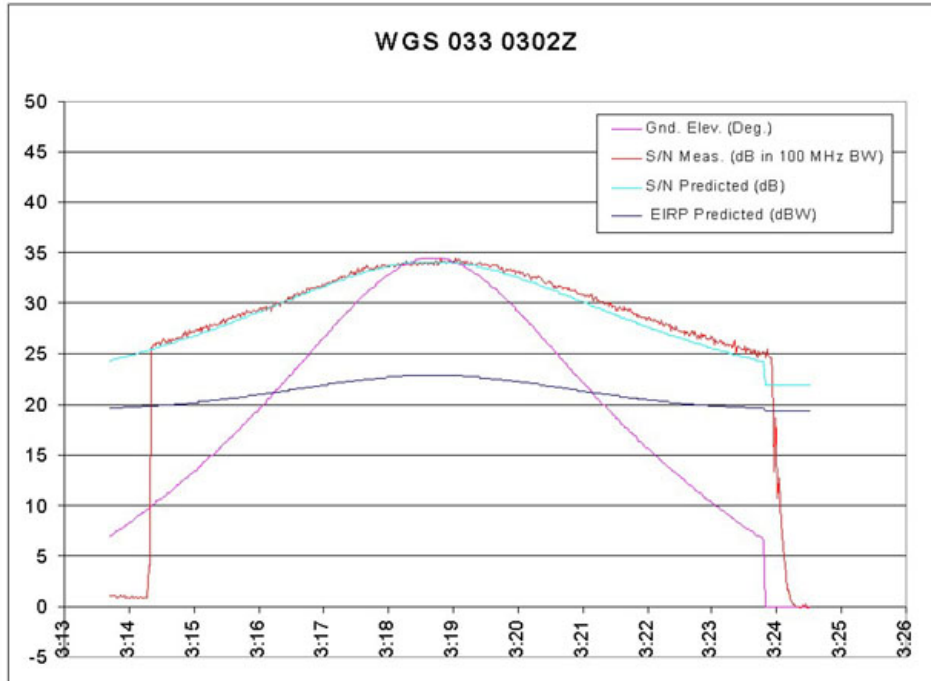


Figure 26. Predicted and actual signal-to-noise ratios at the Wallops ground station during an EO-1 pass. The predicted level includes adjustments for slant range and EIRP variation of the XPAA due to scan angle.

3.5 Validation of the Performance and Reliability of the Electronics and Software

The XPAA provided telemetry consisting of mode and pointing angle information, various internal voltages, temperatures, and currents that were collected by EO-1's command and data handling system via the MIL-STD-1773 bus and returned to ground via the S-band communications link. Deviations from pre-set bounds were reported to mission controllers either by the XPAA's internal computer (ESN) or ground computers, both of which continuously evaluated this information. In addition, this information was manually compared to pre-launch data to identify trends or gradual degradations that might ultimately lead to a failure. Figures 27-30 depict telemetry from March 2002, which is in all respects identical to data from I&T and early-orbit periods.

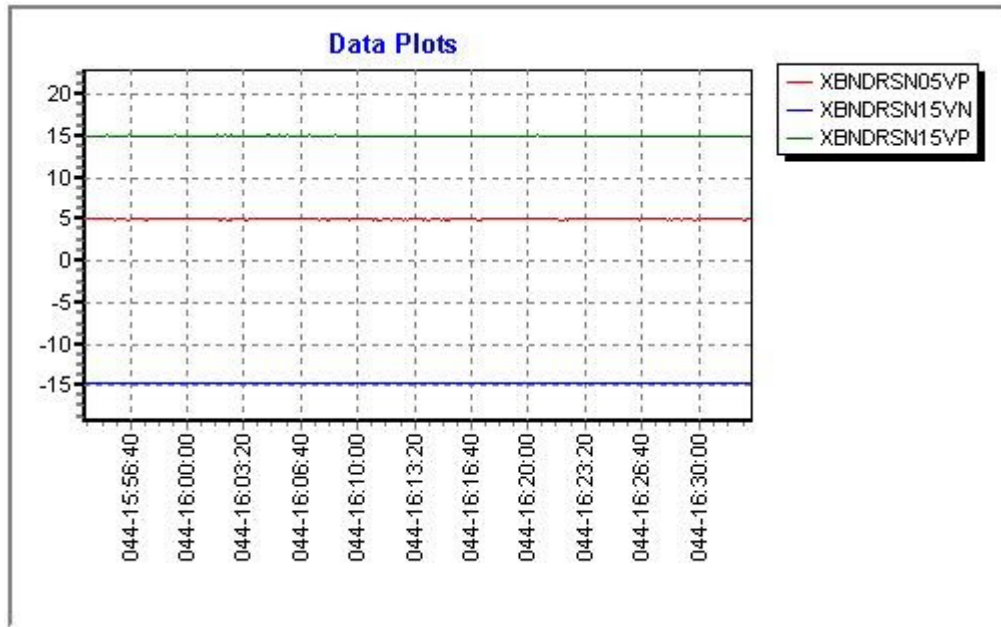


Figure 27. Power supply voltages associated with the Essential Services Node (ESN) processor before, during, and after a downlink event.

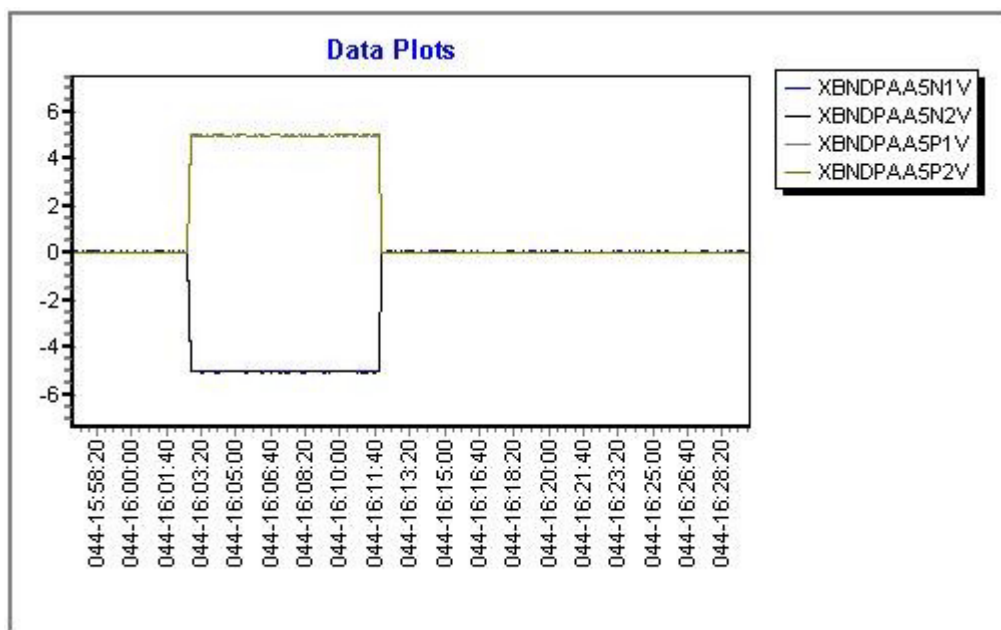


Figure 28. Power supply voltages associated with the XPAA's RF modules before, during, and after a downlink event. These supplies are operative only during actual downlinks.



Figure 29. Power supply currents associated with the XPAA's RF modules before, during, and after a downlink event. These currents are drawn only during actual downlinks. The negative currents are for bias circuits. The positive currents vary with the antenna's pointing angle due to array effects on the elements.

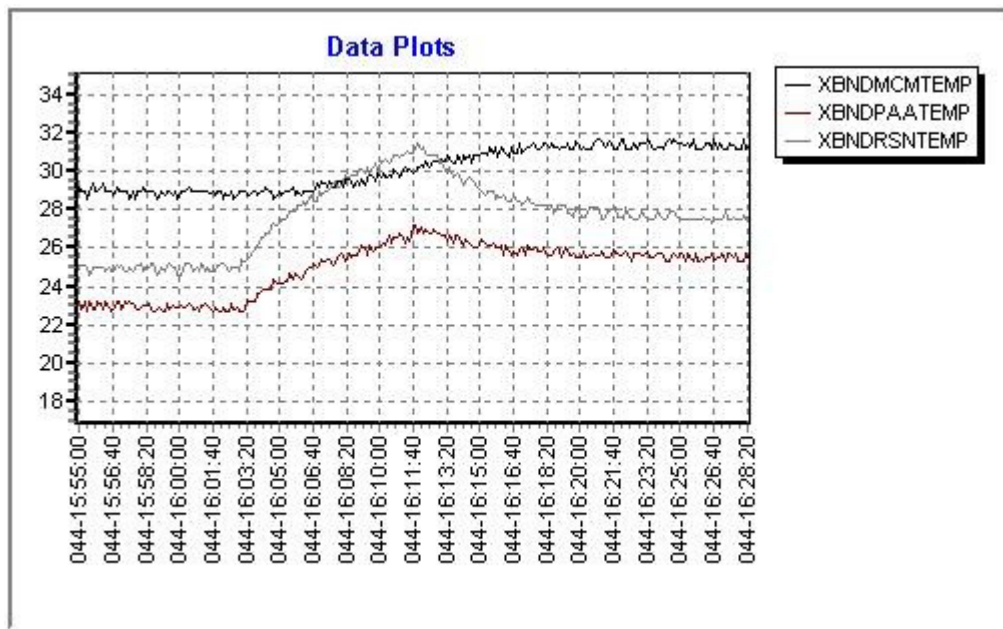


Figure 30. XPA internal temperatures before, during, and after a downlink event.

Throughout the mission, all temperature readings have been consistent with pre-launch predictions. The antenna is typically maintained at a temperature of 25 degrees C, which rises approximately 5 degrees during a downlink event. The ESN multi-chip module (MCM), which operates continuously and is buried in the center of the antenna, typically runs 5-6 degrees C hotter than the RF elements. The antenna baseplate is equipped with heaters to maintain the minimum temperature at 0 degrees C.

The software was verified by comparing XPAA pointing telemetry to commanded angles from the attitude control system. The angle interpolation algorithm in the XPAA was evaluated by comparing on-board interpolated values to see that they were consistent with the ground-commanded angles. Pointing anomalies would have tended to show up in the EIRP contour evaluation or in excessive bit- or burst-error rates at the ground stations. No anomalies were seen which were attributable to the XPAA.

4. TECHNOLOGY TRANSFER AND INFUSION POTENTIAL

Flight of this technology was intended to be a steppingstone toward use of phased arrays in Ka-band, enabling Gigabit data rates from small-to-moderate sized spacecraft.

In addition to the flight X-Band Phased Array described here, engineering model phased arrays Ku-, and Ka-band have been developed by the GSFC Microwave Systems Branch and considered for a number of NASA missions including Next Generation Space Telescope (NGST), National Polar-orbiting Operational Environmental Satellite System Preparatory Project (NPP), X-37, SDO, Landsat follow-on, International Space Station (ISS), and Space Shuttle.

The EO-1 mission has retired much of the perceived technology risk associated with phased array, showing that the technology has advantages that can reduce cost in the spacecraft I&T phase. Acquisition cost continues to be the major factor in final project decisions, but costs for phased arrays are approaching those of traditional systems as the technology continues to mature.

5. LESSONS LEARNED

Near field scanning proved to be a valuable and reliable technique for trending antenna performance throughout the mission life cycle. It was used to verify that the XPAA performed in a consistent manner throughout the spacecraft integration process. It was also used to verify the end-to-end performance of the EO-1 X-band communications system, verifying that the antenna pointed where the attitude control system told it to.

The I&T phase of this technology was in general smooth and trouble-free. Some new design features were identified which could further streamline those processes. For example, using independently switched antenna elements in future arrays would provide the ability to verify their health individually, without the need to use the near field holograms. Similarly, an enhanced test hood with multiple RF pickups could potentially be used to verify antenna pointing. These changes could substantially reduce the amount of near field scanning that is required to verify the antenna's performance.

The X-band anomaly Tiger Team recommended that compatibility tests for new technologies such as the XPAA should include all aspects of the link with the ground station, including ground antenna tracking.

A pre-planned pointing diagnostic test in software should be implemented in the phased array. This would have made on-orbit verification of antenna pointing much easier. Such a test was implemented in GRC's developmental Direct Data Downlink phased array.

Fabrication and testing of Teflon multilayer PWBs required special attention. The XPAA's main circuit board, containing RF and digital traces, required numerous plated-thru holes (vias). Drilling these vias cleanly

through the microwave substrate was a significant challenge. In fact, the boards flown in the antenna required a quality control waiver because test coupons could not pass their “clean vias” examination.

6. CONTACT INFORMATION

Kenneth L. Perko
NASA Goddard Space Flight Center
Code 567
Greenbelt, MD 20771
Telephone: 301-286-7665
Email: kenneth.l.perko.1@gsfc.nasa.gov

7. VALIDATION SUMMARY

This report has presented a summary of the results from validation testing of the X-Band Phased Array Antenna on EO-1. Throughout the antenna’s delivery, integration and test, and flight phases, the antenna met or exceeded all EO-1 requirements. This technology was shown to be fully space qualifiable and compatible with GSFC integration and test practices. The EO-1 mission has validated that phased array antenna of this type are reliable and fully compatible with the NASA ground network.

Throughout the first year of on-orbit operation, the XPAA has been operated at a rate more than five times the original requirement, without difficulty. All tests show a consistent performance throughout the life cycle of the antenna. Final measurements of the array on-orbit using a ground station have provided data that is consistent with the pre-launch results, confirming the successful end-to-end RF performance of the XPAA.

By all measures made so far, the XPAA is performing flawlessly. It was designed to meet a requirement of one downlink per day, delivering 40 Gigabits per day to the ground. The EO-1 project is currently receiving more than 160 Gigabits of data per day during 4-5 downlinks via the X-band system.

8. ACKNOWLEDGEMENTS

The authors would like to thank Larry Winslow of Boeing for his unfailing support for the program. Bill Jupin from Litton/Amecom provided invaluable technical assistance in testing the XPAA after its delivery, as did GSFC’s Dave Israel, who provided the Specviewer and Specdata programs. John Demas and Allen Newell, of NSI Inc., provided enthusiastic on-site support and consultation with near field scanning technology and methods.

The members of the Tiger Team that helped iron out the X-band ground station issues in the first months after launch included Art Azarbarzin, Deane Charlson, Frank Stocklin, Garry Fisher, Dan Mandl and Paul Garza (GSFC); Richard Kunath (GRC); J.R. Hendrickson (Consolidated Space Operations Contract - CSOC); Bob Rodriguez (Honeywell); Wayne Rohr (Litton/Amecom); and Jim Takeuchi (Boeing).

We would also like to thank Larry Alexander for his regular and reliable service in running the AMPEX recorder during many GSFC passes, Kelvin Brentzel and Dan Jacob for maintaining a smoothly-running ground station at GSFC, Robert Bote and the EO-1 support team for scheduling regular passes and Mike Perry and Joe Damiano for coordinating the temporary shutdown of their terrestrial X-band link.

9. REFERENCES

- [1] Dan Slater, "Near Field Antenna Measurements," Artech House, Boston, 1991
- [2] Allen C. Newell, Robert D. Ward and Edward J. McFarlane, "Gain and Power Parameter Measurements Using Planar"
- [3] NASA Contract Number NAS5-97159, New Millennium Earth Observer 1 X-Band Phased Array Antenna
- [4] Huggins, R.W., et al., "Phased Array Transmit Antenna for a Satellite," IEEE Trans-AP, Vol. 1, 1999

ACRONYMS and ABBREVIATIONS

ADT	Architecture Design Team	LHC	Left-hand Circular
AFB	Air Force Base	LNA	Low-Noise Amplifier
AGC	Automatic Gain Control	LO	Local Oscillator
ASIC	Application-Specific Integrated Circuit	LPT	Limited Performance Test
ASM	Attached Sync Marker	Mbps	Millibits per second
BER	Bit Error Rate	MCM	Multi-Chip Module
C	Celsius	MHz	megahertz
C/N	Carrier-to-Noise	MIL-STD	Military Standard
CADU	Channel Access Data Unit	MMIC	Monolithic Microwave Integrated Circuit
CCSDS	Consultative Committee for Space Data Systems	NF	Near Field
CPT	Comprehensive Performance Test	NGST	Next Generation Space Telescope
CSOC	Consolidated Space Operations Contract	NMP	New Millennium Program
dB	Decibel	NPP	National Polar-orbiting Operational Environmental Satellite System Preparatory Project
dBW	Decibel-Watts	NRZ-L	Non-Return to Zero - L
dBm	Decibel-Milliwatts	NRZ-M	Non-Return to Zero - M
EEPROM	Electronically Erasable Programmable Read Only Memory	NSI	Near Field Systems, Inc.
EIRP	Effective Isotropic Radiated Power	PAE	Power Added Efficiency
EMI/EMC	Electromagnetic Interference/ Electromagnetic Compatibility	PN	Pseudo-Random Noise
EO-1	Earth Observing-1	PWB	Printed Wiring Board
ESN	Essential Services Node	Q	Quadrature
FPGA	Field Programmable Gate Array	QPSK	Quadrature Phase Shift Key
GGG	Goddard Ground Station	RF	Radio Frequency
GPIB	General Purpose Interface Bus	RSN	Remote Services Node
GPS	Global Positioning System	SCR	Silicon-Controlled Rectifier
GRC	Glenn Research Center	SDO	Solar Dynamics Observatory
GSFC	Goddard Space Flight Center	SEL	Single-Event Latchup
I	In-phase	SSDIF	Spacecraft Systems Development and Integration Facility
I&T	Integration and Test	SSPA	Solid-State Power Amplifier
I/O	Input/Output	SWG	Science Working Group
IF	Intermediate Frequency	TID	Total Ionizing Dose
IPDT	Integrated Product Development Team	VCDU	Virtual Channel Data Unit
ISS	International Space Station	VDC	Volts-DC
JPL	Jet Propulsion Laboratory	WAIM	Wide-Angle Impedance Matching
krad (Si)	Radiation Dose - kilo-Rads in Silicon	WARP	Wideband Advanced Recorder Processor
		XPAA	X-Band Phased Array Antenna

Appendix A - EO-1 Quadrature Differential Design (Gray code)

The quadrature differential code is most easily understood by first considering the RF signal received by the decoder.

- When there is no phase change, 0° , from one symbol period to the next, both the I and Q channel data is 0.
- When there is a phase change of 180° from one symbol period to the next, both the I and Q channel data is 1.
- When the phase change from one symbol period to the next is $+90^\circ$, the I channel data is 0 and the Q channel data is 1.
- When the phase change from one symbol period to the next is -90° , the I channel data is 1 and the Q channel data is 0.

The purpose of the *encoder* is to output the correct bits (i,q) to cause a standard modulator to create the phase shifts described above. In order to do this for a given input bit pair (a,b), the previously output pair (i(k-1),q(k-1)) must be considered. For example, if the current data is (1,1), an 180 deg phase shift must be applied to the carrier. If the previous data bits were (1,0) then the encoder must put out a (0,1) so that the modulator will change the carrier phase from 135 deg to 315 deg.

Table A-1. EO-1 Gray Code and Quadrature Differential Encode Format

I data	0	1	0	1	
Q Data	0	0	1	1	$\frac{1\ 0}{1\ 1} \mid \frac{0\ 0}{0\ 1}$
Phase	045	135	315	225	

Input Data		Previous Output Data		Output Data		Output Δ Phase
a(k)	b(k)	i(k-1)	q(k-1)	i(k)	q(k)	$\Delta\Phi$
0	0	0	0	0	0	0°
0	0	0	1	0	1	
0	0	1	0	1	0	
0	0	1	1	1	1	
0	1	0	0	1	0	$+90^\circ$
0	1	0	1	0	0	
0	1	1	0	1	1	
0	1	1	1	0	1	
1	0	0	0	0	1	-90°
1	0	0	1	1	1	
1	0	1	0	0	0	
1	0	1	1	1	0	
1	1	0	0	1	1	180°
1	1	0	1	1	0	
1	1	1	0	0	1	
1	1	1	1	0	0	

Appendix B – Distribution of Errors Per Bin

The 26,250 bins have different number of errors inside for each data set. The tables below show how many bins have errors within a certain range. For instance, there are 16 out of 26,250 bins that have 0-3 errors in BER2. There are 254 bins that have 4-6 errors for BER2. The expected distributions are Gaussian for all the data sets except BER2 and CTL for which the calculated distributions are Poisson.

	BER 2			BER 3			BER 4			BER 5	
Xrange	Expect	Observe									
3	0.08	16	24	88.07	58	24	76.81	37	931	0.60	1
6	6.17	254	28	184.20	178	28	156.55	160	952	2.96	5
9	117.66	513	32	457.23	490	32	386.30	361	973	14.13	10
12	856.06	2514	36	970.42	1159	36	822.87	953	994	55.93	49
15	2998.34	2480	40	1761.04	2076	40	1513.14	1800	1015	183.57	184
18	5819.79	5953	44	2732.59	3072	44	2402.04	2814	1036	499.73	518
21	6882.63	3469	48	3625.64	3853	48	3291.84	3655	1057	1128.31	1154
24	5310.43	5378	52	4113.38	4187	52	3894.56	4060	1078	2112.95	2119
27	2815.30	2075	56	3990.45	3733	56	3977.79	3699	1099	3282.04	3354
30	1068.02	2268	60	3310.19	2945	60	3507.43	3180	1120	4228.65	4257
33	299.58	605	64	2347.95	2119	64	2669.91	2349	1141	4519.25	4505
36	63.83	530	68	1424.05	1221	68	1754.55	1512	1162	4006.29	3991
39	10.57	110	72	738.51	634	72	995.38	864	1183	2945.93	2871
42	1.39	66	76	327.46	314	76	487.48	459	1204	1796.82	1760
45	0.15	10	80	124.15	143	80	206.09	217	1225	909.02	906
48	0.01	8	84	40.24	50	84	75.21	83	1246	381.43	375
51	0.00	1	88	11.15	11	88	23.70	32	1267	132.74	130
54	0.00	0	92	2.64	5	92	6.44	12	1288	38.31	41
57	0.00	0	96	0.54	0	96	1.51	2	1309	9.17	16
60	0.00	0	100	0.09	2	100	0.31	1	1330	1.82	4

	BER 6			BER 7			CTL	
Xrange	Expect	Observe	Xrange	Expect	Observe	Xrange	Expect	Observe
1774	6.16	4	860	0.42	0	1	26187.40	25798
1796	18.28	16	880	2.31	2	2	61.14	428
1818	59.89	52	900	11.99	13	3	1.44	19
1840	169.37	179	920	50.90	42	4	0.03	5
1862	413.36	391	940	176.94	172	5	0.00	0
1884	870.63	902	960	503.34	522	6	0.00	0
1906	1582.58	1675	980	1171.93	1172	7	0.00	0
1928	2482.72	2522	1000	2233.33	2231	8	0.00	0
1950	3361.45	3333	1020	3483.72	3582	9	0.00	0
1972	3927.93	3891	1040	4448.21	4623	10	0.00	0
1994	3961.36	3949	1060	4649.28	4559	11	0.00	0
2016	3447.99	3450	1080	3977.84	3944	12	0.00	0
2038	2590.16	2544	1100	2785.89	2665	13	0.00	0
2060	1679.29	1676	1120	1597.08	1559	14	0.00	0
2082	939.63	909	1140	749.40	715	15	0.00	0
2104	453.74	478	1160	287.81	304	16	0.00	0
2126	189.09	195	1180	90.47	109	17	0.00	0
2148	68.01	54	1200	23.27	27	18	0.00	0
2170	21.11	26	1220	4.90	7	19	0.00	0
2192	5.65	4	1240	0.84	2	20	0.00	0

Appendix C – EO-1 X-Band Link Budgets

XPAA Downlink Budgets	Radarsat Equivalent Link as Flown	Originally Designed Link Budget
Spacecraft Characteristics		
Data Rate (kbps) QPSK	105000.00	150000.00
Carrier Freq (MHz)	8225.00	8225.00
Transmitter Power (Watts)	3.20	3.20
Transmitter Power (dBm)	35.05	35.05
Pointing Loss (dB)	-0.25	-0.25
Passive Losses (dB)	-0.50	-0.50
Ohmic Loss	-0.50	-0.50
Scan Loss	-4.51	-4.51
Impedance Mismatch (2.0:1) VSWR	-0.50	-0.50
Transmit Antenna Gain (dB)	23.30	23.30
EIRP (dBm)	52.09	52.09
Transmission Medium		
Range (km)	1677.00	1677.00
Free Space Dispersion (dB)	-175.23	-175.23
Modulation Loss (dB)	-0.40	-0.40
Polarization Loss (dB)	-0.35	-0.35
Atmospheric (dB)	-0.69	-0.69
Rain Atten (dB)	-1.30	-1.30
Scintillation Loss (dB)	-0.30	-0.30
Total Path Loss (dB)	-178.27	-178.27
Receiver Characteristics		
Ground Antenna Diameter (m)	11.00	9.00
Ground Antenna Efficiency	0.55	0.55
Ground Antenna Gain (dB)	56.93	55.19
Pointing Loss (dB)	-0.50	-0.50
Received Power (dBm)	-69.75	-71.49
System Noise Temp (K)	150.00	150.00
Receive System G/T (dB)	35.17	33.43
Data Rate (dB-bps)	80.21	81.76
System Noise (dBm)	-96.63	-95.08
Available SNR (dB)	26.88	23.58
Req'd C/N for BER (dB)	13.55	13.55
Implementation Loss (dB)	-5.00	-5.00
Coding Gain (dB)	1.90	1.90
Required Margin (dB)	0.00	0.00
Signal Margin (dB)	10.22	6.93

Appendix D – EO-1 X-Band Coordinate Reference Frames

